An-Najah National University

Faculty of Graduate Studies

DESIGN, SYNTHESIS, AND BIOLOGICAL EVALUATION OF THIAZOLE-CARBOXAMIDE DERIVATIVES AS COX INHIBITORS

By

Rozan Ghassan Sabobeh

Supervisors

Dr. Nidal Jaradat

Dr. Mohammed Hawash

This Thesis is Submitted in Partial Fulfillment of the Requirements for the Degree of Master of Pharmaceutical Sciences, Faculty of Graduate Studies, An-Najah National University, Nablus - Palestine.

2022

DESIGN, SYNTHESIS, AND BIOLOGICAL EVALUATION OF THIAZOLE-CARBOXAMIDE DERIVATIVES AS COX INHIBITORS

By

Rozan Ghassan Sabobeh

This Thesis was Defended Successfully on 26/12/2022 and approved by

Dr. Nidal Jaradat	
Supervisor	Signature
Dr. Mohammed Hawash	
Co-Supervisor	Signature
Dr. Fuad Al-Rimawi	
External Examiner	Signature
Dr. Mohyeddin Assali	
Internal Examiner	Signature

Dedication

To my wonderful husband who was the main supporter and the source of my strength always and forever.

To the one who made me a mom, my firstborn.

To my parents for raising me to believe that nothing is impossible and a persons' will be stronger than any obstacle in the presence of certainty in God, they are my backbone and still are.

To my dear sisters

To the supervisors who deserve their scientific degree, I am proud that I was their student.

To my colleagues at work who supported me.

To everyone who loves me and is happy about my success

I dedicate this work

Acknowledgement

I would like to thank the supervisors of my thesis. The main supervisor, Dr. Nidal Jaradat, always motivates me and helps me use my abilities in the right place. I would also like to thank my Co-supervisor, Dr. Mohamed Hawash, who followed up on my work with his gentle dealing and was always available when I faced a problem and needed his advice during work. He taught me to rely on myself and guided me on the right way to achieve.

Thanks to Dr. Mohammed Qaoud from Gazi University, Ankara, Turkey, for helping in the molecular docking study.

Special thanks to the staff of the laboratories of the College of Pharmacy for their help, especially Tahreer Ishtayeh.

Finally, my family and my husband deserve a big thanks for their real support and faith in my abilities; without their support, I would not be able to achieve my goal.

Declaration

I, the undersigned, declare that I submitted the thesis entitled:

DESIGN, SYNTHESIS, AND BIOLOGICAL EVALUATION OF THIAZOLE-CARBOXAMIDE DERIVATIVES AS COX INHIBITORS

I declare that the work provided in this thesis, unless otherwise referenced, is the researcher's own work, and has not been submitted elsewhere for any other degree or qualification.

Student's Name: _____

Signature: _____

Date: _____

List of Contents

List of Tables

List of Figures

List of Appendices

DESIGN, SYNTHESIS, AND BIOLOGICAL EVALUATION OF THIAZOLE-CARBOXAMIDE DERIVATIVES AS COX INHIBITORS

By

Rozan Ghassan Sabobeh

Supervisors

Dr. Nidal Jaradat

Dr. Mohammed Hawash

ABSTRACT

Non-Steroidal anti-inflammatory drugs (NSAIDs) are often employed to alleviate swelling and discomfort and lower high temperatures. They inhibit the cyclooxygenase enzyme (COX) required to convert arachidonic acid to Prostaglandins that are inflammatory. In this master's thesis, new thiazole derivatives with aniline derivatives were synthesized, specified, and estimated for their selectivity and potency at COX-1 and COX-2 by an in vitro COX inhibition assay kit. The synthesized compounds' cytotoxicity was estimated using an MTS assay against human hepatic stellate (LX-2) and the normal cell line (Hek293T). HRMS, 1H-NMR, and 13C-NMR techniques characterized all newly synthesized chemicals. The results demonstrated that the most effective compound against the COX-1 enzyme was 2b with an IC_{50} =0.239 µM. It also showed potent activity against COX-2 with IC_{50}=0.191 µM with a selectivity ratio of 1.251. The highest selectivity ratio was (2.766) for 2a compound against COX-2 with an IC_{50} = 0.958 µM relating to celecoxib ratio (23.8) and its IC_{50} against COX-2 =0.002 µM. The 2j compound also showed good selectivity towards COX-2 (1.507) with an IC_{50} of 0.957 µM. All compounds showed negligible cytotoxic activity against the evaluated normal cell lines, and the IC_{50} values were more than 300 µM, except compound 2b**,** whose IC_{50} values were 203.711.89 and 116.96±2.05 µM against LX-2 and Hek293t cell lines, respectively.

Keywords: Anti-inflammatory; Cyclooxygenase enzyme; COX inhibitors; Docking studies; Heterocyclic; Thiazole-carboxamide; NSAIDs.

Chapter One

Introduction

1.1 Introduction

This thesis documents several key contributions made in the field of NSAIDs. A five-membered heterocyclic compound called thiazole. compound with nitrogen and sulfur atoms, plays an important function in medicinal chemistry. It is considered a major component in numerous natural (vitamin B1) and synthetic medicinal compounds. The diversity of the thiazole nucleus appears because it is an important part of the penicillin nucleus, and some of its derivatives have exhibited antifungal (abafungin), antimicrobial, and antihistaminic activity. Regarding the synthetic significance of thiazole derivatives, they have condensed forms and reduced derivatives that have grown as a result of their new applications as anthelmintic and anticancer [1].

Heterocyclic substances are organic cyclic substances that include at least one distinct atom. Nitrogen and oxygen are the most common heteroatoms [2]. Important to realize that Heterocyclic compounds have the largest diverse family of organic compounds. Many of them are known these days, and the number is increasing continuously. Additionally, they also have a main role in science fields such as biochemistry and medicinal chemistry. Due to the relationship between medical difficulties and chemistry, the study of the most prevalent illnesses and the best ways to treat them has made medicinal chemistry a significant subfield of chemistry. When active compounds were first isolated and purified from animal and plant tissues, this area of chemistry was born, and it has since drawn the interest of researchers all over the globe.

Regarding biological implications of heterocycles, they are found in many biomolecules like vitamins, enzymes, and physiologically active substances, including anti-inflammatory, antifungal, enzyme inhibitors, antibacterial, anti-HIV, antioxidant, herbicidal, and anticancer activities. Regarding the antifungal activity, the antifungal medicine effect kills the fungal cells due to the effect on the substances present in the cell membrane that leads to cell component leakage and cell death. Another way is by limiting the development of fungal cells and reproduction. Anti-inflammatory activity reduces inflammation and pain sedation compared to opioids, which act on the CNS to inhibit the brain's pain-signaling pathways. Aspirin, naproxen, and ibuprofen are the

most used anti-inflammatory drugs called Non-steroidal Anti-inflammatory Drugs (NSAIDs). A phrase used to describe medications that used in therapy or prevention of bacterial illnesses is "antibacterial activity of antibiotics". Antibiotics do not affect viral infections such as influenza or the common cold, and inappropriate use of antibiotics causes resistant organisms. Aromatic heterocyclic derivatives are considered a crucial component of antibiotics' chemical structure, such as β-lactam derivatives [3].

Even after the development of selective COX-2 inhibitors, NSAIDs are still widely used medications [4]. They are a drug class FDA-approved as anti-inflammatory, antipyretic, and analgesic agents. These uses making NSAIDs practical for treating dysmenorrhea, arthritic conditions, muscle pain, gout, and migraines [5]. NSAIDs have negative side effects that are mediated by prostaglandin synthesis inhibition from arachidonic acid via non-specific blocking of cyclooxygenase enzyme causing vasoconstriction [4]. The two major categories of NSAIDs are selective COX-2 inhibitors, which are more recent, and non-selective NSAIDs, which are both COX-1 and COX-2 inhibitors. Aspirin is a non-selective NSAID that is primarily used for its antiplatelet effects, which lower the risk of cardiac re-infarction. Prostaglandins (PGG2 and PGH2) are produced when arachidonic acid is processed by the cyclo-oxygenase isoenzymes COX-1 and COX-2. These prostaglandins act as mediators of inflammation, fever, and pain. Prostacyclin induces vasodilation, thromboxane A2 stimulates platelet aggregation, and NSAIDs prevent the production of prostaglandins, thromboxane A2, and prostacyclin by inhibiting COX enzymes. The therapeutic applications of NSAIDs largely rely on their enzyme selectivity [6].

Examples of FDA-approved NSAIDs:

-Non-selective NSAIDs:

- Ibuprofen
- Indomethacin
- Ketoprofen
- Diclofenac
- Meloxicam
- Piroxicam

- Sulindac
- Naproxen

- COX-2 Selective NSAIDs such as Celecoxib.

Figure 1.1

Examples of FDA-approved NSAIDs [7-9]

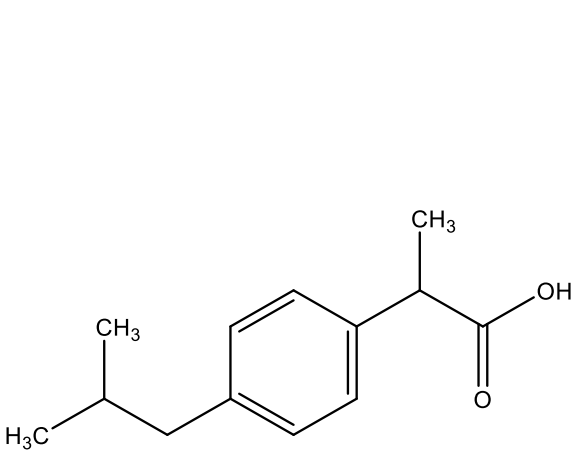

Ibuprofen

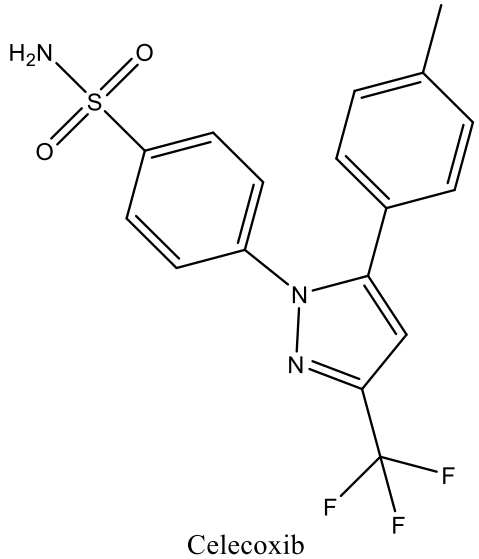

Celecoxib

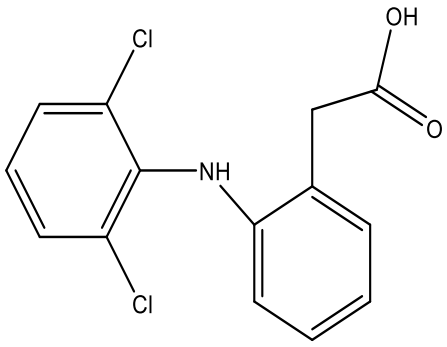

Diclofenac

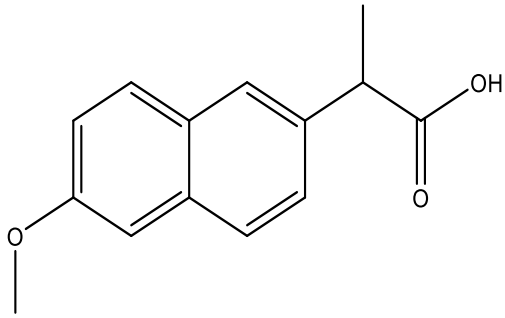

Naproxen

According to dosage, NSAIDs oral tablets are the most prevalent form for the most known over-the-counter NSAIDs such as aspirin regular strength,1 to 2 tablets every 4 hours, or Aspirin has a daily maximum dose of 4000 mg, which may be taken as 3 pills every 6 hours of 325 mg strength. Additional topical NSAIDs, such as diclofenac sodium 1.5% topical solution, are available. They are most beneficial in osteoarthritis and pain treatment because of soft-tissue damage. Particular NSAIDs may also parenterally administered. For instance, ibuprofen is administered intravenously as a 30-

minute infusion. NSAIDs frequently cause side effects, including bad effects on the stomach, which are because of the blocking of COX-1 that prevent the process of making prostaglandins which shield the mucosa of the stomach, cardiovascular and unfavorable renal effects are due to COX-1 and COX-2 that help in the production of prostaglandins which play an important function in renal hemodynamics [5].

Thiazole is considered an ideal pharmacophore nucleus because of its numerous pharmaceutical applications and biological activities like anti-inflammatory, antibacterial, anti-allergic, and anti-cancer. There are several ways for thiazole derivatives synthesizing, such as the following synthesis methods:

- Hantzsch (1889) is the main method and refers to the reactions of α-halo carbonyl compounds with thiourea or thioamides. This mechanism includes the nucleophilic attack (thioamide sulfur atom) on the alpha-halo carbonyl (alpha carbon), with additional dehydration leading to the same thiazole and the creation of an intermediate. One option to change this process is to concentrate 1,2-dichloro-1-ethoxyethane using thiourea or its derivatives.

- Cook–Heilbron method produces 2,4-disubstituted 5-aminothiazole derivatives when aminonitrile and carbon disulfide combine.

- Robinson–Gabriel's method involved cyclizing acylamino carbonyl compounds with stoichiometric amounts of phosphorus pentasulfide.

- Reduction of methylthiothiazole to synthesize thiazole.

- New ways for making thiazole derivatives, such as making 5-arylthiazoles by treating N, N-diformylaminomethyl aryl ketones with phosphorus pentasulfide and triethylamine in chloroform. A good yield of 5-arylthiazoles is produced as a consequence of the reaction.

- Thiazoles synthesis from anhydrides, oximes, and KSC.

- Thiazoles synthesis from amines, aldehydes, and elemental sulfur.

- Thiazoles synthesis by isocyanide cyclization with methyl arene- and hetarenecarbodithioatesa.

- Variable response circumstances Utilizing vinyl azides and potassium thiocyanate, create thiazoles.

- Thiazoles synthesis from sulfonyl-1,2,3 –triazoles, and thionoesters.

- Thiazoles synthesis from α-bromoketones and thiosemicarbazones under microwave radiation [10].

1.2 Biological activities of thiazoles

Thiazoles are found in numerous effective biological compounds, such as Abafungin (an antifungal drug), Ritonavir (an antiretroviral drug), and Sulfathiazole (an antimicrobial drug). It has been noted thiazole compounds have a variety of biological actions throughout the years, including anti-inflammatory properties, anti-schizophrenia, antihypertensive, antibacterial, and analgesic activity [11].

Recently, because of the advent of bacterial strains that are resistant to many drugs such as Enterococcus sp, Enterobacter cloeacae (E. cloacae), Pseudomonas aeruginosa (P. aeruginosa), Acinetobacter baumannii (A. baumani), Candida sp and Staphylococcus aureus, medicinal chemists have recently focused on designing and developing antimicrobial agents with various mechanisms of action [12].

Several 2-alkyl/arylamino 5-((6-(4 bromo phenyl) imidazo [2,1-b] thiazol-3-yl) methyl) Derived from 1,3,4-thiadiazoles were synthesized by Guzeldemirci and Kucukbasmac (2010), and the antimicrobial efficiency were tested for several compounds by micro broth dilution technique, 5-(6-(4-bromophenyl) imidazo[2,1-b] thiazol-3-yl) methyl)-Nphenyl-1,3,4-thiadiazol-2-amine observed good antimicrobial properties.

Holla and colleagues (2008) created a number of new 4-aryl/ chloroalkyl-2- (2,3,5-trichlorophenyl) 1,3-thiazoles derivatives and evaluated the potency of each one as an antibacterial (2,3,5-trichlorobenzylidene) 2-(4-nitrophenyl)thiazole-2-yl)hydrazine and 2- (2,3,5-trichlorophenyl) -4-(4-substituted-phenyl) E. coli and Pseudomonas aeruginosa responded well to thiazole treatment.

In order to test the anti-inflammatory action, Rostom et al. (2009) synthesized a number of polysubstituted thiazole derivatives and used formalin-induced paw edema to measure the activity. 4-phenylthiourea-2-, a common medication, and diclofenac sodium (dicyanomethylene) -2,3-dihydro-N-(2,5-dihydro-2,3-dimethyl-5-oxo-1-phenyl-1H-pyrazol-4-yl) The compounds 4-amino-2-(3-phenylthiazole-5-carboxamide) and (dicyanomethylene) -2,3-dihydro-N-(2,5-dihydro-2,3-dimethyl-5-oxo-1-phenyl-1H-pyrazol-4-yl) Analgesic and anti-inflammatory effects of 3-phenylthiazole-5-carboxamide were shown, and they had a quick start.

Devasagayam et al. (2008) proved the antioxidant efficacy of aminothiazole derivatives ([(4-amino-5-benzoyl2-(4methoxyphenyl amino) thiazole]) which are called dendrodoine analogs. A number of thiazolidinone and thiazoline derivatives with sydnonyl substitutions were created by Shih et al. in 2004 and screened them for their antioxidant performance. They showed high antioxidant action since they had a significant amount of DPPH (1,1-diphenyl-2-picrylhydrazyl) free radical scavenging activity compared to vitamin E. In order to test for their diuretic effect, Andreani et al. (1987) developed a group of imidazo [2,1-b] thiazole acetohydrazones. Imidazo[2,1-b] thiazole acetohydrazones' 2-methyl derivative, which, when tested, has a phenyl ring at position C-6 and had a potent diuretic effect [11].

Figure 1.2

examples of thiazole derivatives which having a biological activity

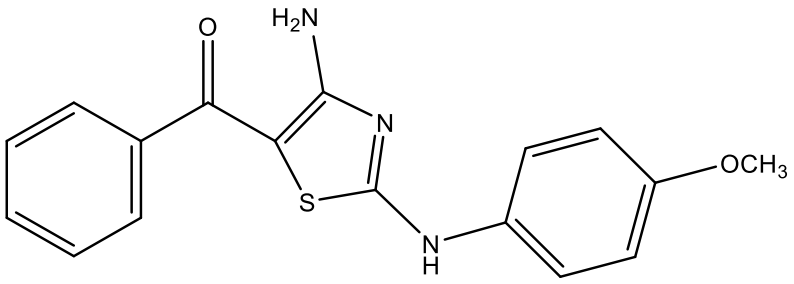

[(4-amino-5-benzoyl2-(4methoxyphenyl amino) thiazole]

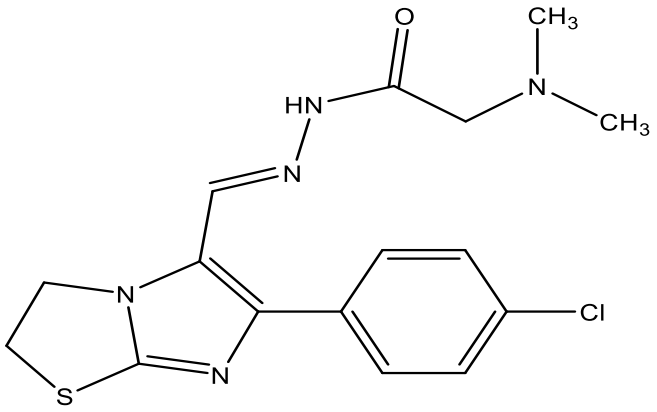

Imidazo[2,1-b] thiazole acetohydrazones

1.3 Similar structures

1.3.1 Imidazo[1,2-b] thiazoles derivatives

It is a hybridized heterocyclic system that includes a bridgehead atom of nitrogen. These modifications to this scaffold are particularly important in medicinal chemistry due to a lot of biological activities.

Figure 1.3

Several compounds of imidazo[1,2-b] thiazole (1)

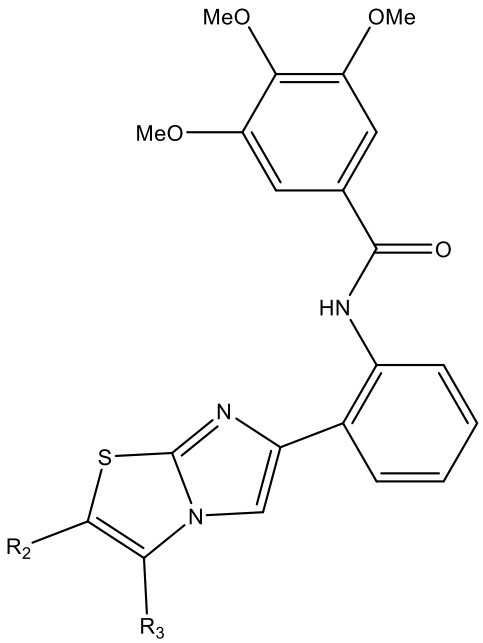

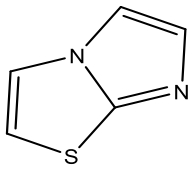

(1)

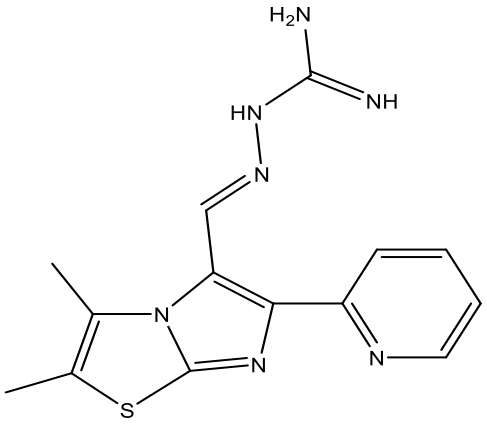

(2)
Decreases mitochondrial membrane potential.

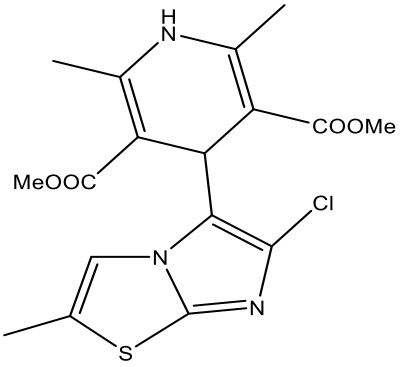

(3)
Selective negative inotropic activity.

Through the last decades, some chains of imidazo[2,1-b] thiazole derivatives were created and showed activity versus different cancer cell lines. Also, the inhibitor of Complex III of the mitochondrial respiratory series was found in the guanylhydrazone derivatives containing the imidazo[2,1-b]thiazole, triggering apoptosis in the cell lines HT29 and HL60 [13].

Modifying different cellular processes like stress response and energy metabolism occurs in response to various environmental catalysts that cause SIRT1 immediately binds the cellular metabolic condition to the chromatin structure and gene regulation expression. SIRT1 is the most protected mammalian NAD^+ - dependent protein deacetylase that has been shown as a metabolic sensor in different metabolic tissues. Modern studies have exhibited that SIRT1 monitors glucose and lipid metabolism in the liver, insulin secretion monitoring in the pancreas, and senses the availability of nutrients in the hypothalamus [14].

A sequence of derivatives of the imidazo[1,2-b] thiazole plays a major role in activating the NAD^+ - dependent deacetylase SIRT1. The water-solubilizing group had an appropriate combining ability at the C-2 or C-3 position of the imidazo[1,2-b] thiazole ring. The activity of the SIRT1 enzyme could be modulated by changing the amide part of these imidazo[1,2-b] thiazole derivatives, seven sirtuins (SIRT1–SIRT7) that are part

of the histone deacetylase (HDACa) family usually mentioned to as class III HDACs. SIRT1 is the most differentiated member of the family, stimulating protein deacetylation to produce nicotinamide. O-acetyl-ADP-ribose happens when SIRT1 uses nicotinamide adenine dinucleotide (NAD+). Recently published articles have found an essential linkage between SIRT1 and different metabolic functions that could probably affect life in rodents and smaller organisms. Two common series of SIRT1 activation are the up-regulation of PGC-1alpha and the increase in mitochondrial biogenesis [15]. SIRT1 signaling passageway could develop mitochondrial biosynthesis to tolerate cardiac and neurological damage. Ginsenoside Rc is one of the active components in *Panax ginseng* [16] and has been recognized for targeting mitochondrial function [17]. Increasing mitochondrial biogenesis causes the development of glucose metabolism in different muscle, adipose, and skeletal tissues, so activation of SIRT1 shares in treating type II diabetes. Mass spectrometry enzymatic assay was utilized to estimate SIRT1 activation. The power was represented as the EC1.5, the chemical dose necessary to enhance 50% more enzyme activity, and the greatest activation percentage that maybe attained at the tested medication's maximum concentrations.

Table 1

Derivatives of imidazo[1,2-b]thiazoles having soluble groups at the C-2 and C-3 positions

Compound	R2	R3	$EC_{1.5}$ (max activation) [a]
4	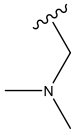	H	4.8 µM (295%)
5	H	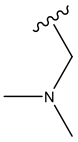	1.9 µM (270%)
6	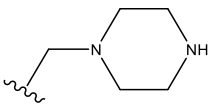	H	3.2 µM (257%)
7	H	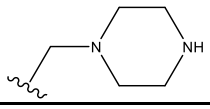	1.8 µM (271%)

In the accompanying table, a list of a few analogs that were developed to explore changes in SIRT1 activity when methylamino derivatives were added to either the C-2 or C-3 position of the imidazothiazole ring [15].

1.3.2 Pyrazole derivatives

A crucial class of five-membered heterocyclic molecules is pyrazoles [18], including two neighboring nitrogen atoms [19]. They constitute the basic structure in many compounds with serious agricultural chemicals and pharmaceutical activities [18]. Pyrazole derivatives have an important function as antitumor agents due to their good inhibition effect versus BRAF (V600E), EGFR, ROS Receptor Tyrosine Kinase, and telomerase. They also have good anti-inflammatory and anti-bacterial actions [20].

These days, pyrazole systems have taken more attention because of their beneficial pharmacological features. This heterocycle is possibly marked in many well-formed drugs being a part of various classes with numerous therapeutic activities [21-23].

Some of the basic procedures of Access to the Pyrazole Nucleus

- Cyclocondensation of Hydrazine and Its Derivatives on 1,3-Difunctional Systems is the main procedure utilized to obtain substituted pyrazoles by a cyclo condensation reaction between suitable hydrazine and a carbon unit such as 1,3-dicarbonyl compound:

a. From 1,3-Diketones: reaction between β-diketone with hydrazine derivatives to give two regioisomers.

b. From Acetylenic Ketones: hydrazine derivatives on acetylenic ketones (cyclo condensation reaction) to produce pyrazoles, the reaction also produces a mixture of two regioisomers.

c. From Vinyl Ketones: In a process known as cyclo condensation,, -ethylenic ketone and a hydrazine derivative create pyrazolines, which are then converted into the pyrazole ring by oxidation.

- Multicomponent Approaches:

a. In Situ Formation of Carbonyl Derivatives: a simple and practical method for making several 1,3-disubstituted compounds from readily accessible chemicals. Terminal alkynes were treated with hydrazines, aromatic aldehydes, and molecular iodine to produce 3,5-substituted pyrazole with a high yield (68-99%) and strong regioselectivity.

b. In Situ Formation of β-Aminoenones: by combining an oxime in dimethylformamide with an alkyne, an unique method for synthesizing 3,5-substituted pyrazoles is enhanced by Kovacs et al., leading to the production of the -aminoenone. Using a straightforward procedure, hydrazine was introduced to the -aminoenone to convert it into pyrazoles; the result was extracted with a 70% yield.

c. In Situ Formation of a Hydrazone: by cyclizing hydrazone dianions with diethyl dioxalate, Dang et al. have described a new process for the synthesis of pyrazole-3-carboxylates that results in a high yield (53%) of the pyrazole-3-carboxylates[24].

Pyrazoles are aromatic molecules because of their planar integrated ring structures with six unspecified location π-electrons. Thus, by comparing them to the characteristics of benzene derivatives, a number of key aspects of these molecules were examined [25]. Regarding the pharmacological significance of pyrazole, Akbas et al. installed a series of 1H-pyrazole-3-carboxylic acid derivatives and estimated their anti-bacterial efficiency versus Staphylococcus aureus, Bacillus cereus, and other strains of bacteria. The findings exhibited antibacterial action versus Gram-positive and Gram-negative germs. A chain of pyrazoles, including a quinolinyl chalcone collection, was created and evaluated for antimicrobial effectiveness. The results showed excellent effectiveness against bacteria and fungi. Another group of pyrazole derivatives was created by synthesis and investigated as selective cyclooxygenase-2 (COX-2) inhibitors. The outcomes showed an important COX-II inhibition (78.91±0.80 %). A series of 1*H*-pyrazolyl derivatives were examined for their anti-inflammatory properties in vivo, showing an excellent selective inhibition versus the COX-2 enzyme. These molecules have also been shown to have anticancer activity, anti-diabetic, anti-Alzheimer's, and anti-Parkinson activities [24].

According to research by Vane, these anti-inflammatory drugs prevent the formation of prostaglandins, which are involved in various physiological and pathological processes, by revealing that the cyclooxygenase enzyme is the therapeutic target of NSAIDs in 1971 [26]. To create a selective COX-2 inhibitor, various diaryl-based pyrazole and triazole derivatives were created and easily produced by Assali et al. (2020). These derivatives were created via various reactions, including the Vilsmeier-Haack and click reactions. Five substances were identified via COX-1 and COX-2 inhibition in vitro investigations as potent and specific COX-2 isozyme inhibitors with IC50 values in the 0.551-0.002 μM range, compound A, a derivative of the diarylpyrazole has an IC50 value of 0.017 μM and the greatest inhibitory action against COX-2 owing to retaining the other aromatic ring unsubstituted while replacing one of the N-aromatic rings with sulfonamide [27].

Figure 1.4

synthesized Pyrazole derivative as a selective COX-2 *inhibitor [27]*

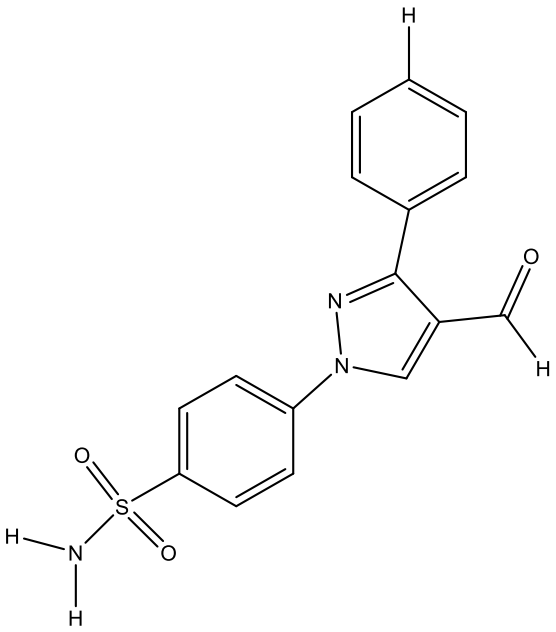

(A)

1.3.3 Pyridine derivatives

Pyridine is considered an organic heterocyclic substance with its chemical formulation C5H5N. Regarding structure, it is related to a benzene ring with a C-H group displaced by a nitrogen atom. Pyridine's name comes from the Greek term, which is the integration of two words, "idine," which is used for aromatic bases, and "pyr," which

indicates fire. Pyridine evolved become a significant target in 1930 with the significance of niacin, a pyridine derivative in treating dermatitis and dementia [28].

In 1876 pyridine was synthesized from acetylene and hydrogen cyanide. Picoline was considered the first pyridine derivative isolated in pure form. The physical characteristics of pyridines result from a stabilized, cyclic, and aromatic structure, including a ring nitrogen atom which has an extra electronegativity than the ring carbons. Therefore, making the two-, four-, and six-ring carbons more electropositive than others would be anticipated from knowledge of benzenoid chemistries [29].

Pyridine derivatives are considered the most common and important heterocyclic compounds, which have significance in different medicinal applications and play important roles in various biological activities, including antifungal, antioxidant, antibacterial, analgesic, and anti-inflammatory activity [30]. Pyridines have a key role in the progress of human medicines, more than 100 medications utilize it, and that number is increasing daily. A lot of academics have been working hard to investigate effective ways to synthesize this skeleton. The most popular methods for making pyridine cores are the Hantzsch, Bönnemann, Bohlmann-Rahtz, and Kröhnke reactions. However, most processes are rarely used because of lacking generality or selectivity and need a costly metal catalyst. N-propargylamines are one of the most significant intermediates in this organic synthesis because of their property as an attractive starting material for different nitrogen heterocycles synthesis. Synthesis of pyridines from N-propargylamines needs simpler conditions and easier procedures than previously mentioned.

Regarding Pyridine synthesis from β-enaminones, N-propargyl and β-enaminones are well-known and one among the most significant intermediates in organic synthesis due to their dual action as electrophiles and nucleophiles. They were effectively turned into different N-heterocycles by both intra- and intermolecular interactions. Pyridine derivatives synthesis could be fulfilled by intramolecular cyclization of available13 N-propargylic β-enaminones. It is worth mentioning that Cacchi and co-workers improved the major work. Those who worked the Cu(I)-catalyzed intramolecular cyclization of a chain of N-propargylic β-enaminones with an environment of argon [31].

1.4 COX-1 and COX-2 overview

The cyclooxygenase (COX) enzymes, which predominantly produce prostaglandin, include the isoforms COX-1 and COX-2. The administration of certain nonsteroidal anti-inflammatory medicines must keep track of prostaglandins since they play important roles in the inflammation process. Selective COX-2 inhibitors were the most commonly used NSAIDs during the coronavirus 2019 pandemic due to their effectiveness in reducing pain and protecting from diseases caused by inflammation [32]. By inhibition, the synthesis of prostaglandins and non-steroidal anti-inflammatory drugs (NSAIDs) make mucosal injury, ulceration, and ulcer complication through the GI tract. Two cyclo-oxygenase enzymes exist, one more prevalent at inflammation locations (COX-2) and the other one basically expressed in the GI tract (COX-1), which has led to the essential therapeutic improvement of COX-2 inhibitors[33]**.** The cyclooxygenase enzyme is thought to be competitively inhibited by NSAIDs. This enzyme serves as an intermediary in the process that turns arachidonic acid into prostaglandins [26]**.**

All NSAIDs block COX-1 and COX-2 in variable ways, and the inhibition mechanism is divided into three classes, but there are exclusions to these classes:

- Class 1: Rapid competition and reversible binding of COX-1 and COX-2, such as ibuprofen.
- Class 2: diclofenac, for example, binds to COX-1 and COX-2 with time-dependent, higher affinity, and slowly reversible binding occurring first. This is followed by quick, lower-affinity, and reversible binding.
- Class 3: rapidly reversible binding followed by covalent alteration of COX-1 and COX-2.

In relation to the production of prostaglandins, NSAIDs block COX-1 and COX-2 and variably modify the synthesis of Thromboxane A2, Prostacyclin, Prostaglandin (PG) [34].

Inflammation and cancer have a recognized connection dating back to the 17th century. Certain types of cancer may be brought on by chronic inflammation. Solid tumors can

start and maintain neighborhood inflammatory reactions that promote the spread and development of tumors [35]. These days, the primary reason for dying is cancer; despite substantial improvements in biology and medical surgery, recent studies have mentioned an essential relationship between the presence of tumors and inflammation. Cyclooxygenase-2 (COX-2) is considered a linker between inflammatory disease and cancer. It was suggested as the main purpose for cancer treatment. However, the major available COX-2 inhibitors, nonsteroidal anti-inflammatory drugs (NSAIDs), have different impacts that are restrict their uses in cancer therapy [36].

As a response to inflammation, prostaglandins are released, which are synthesized from arachidonic acid via COX-1 and COX-2 (the cyclooxygenase enzymes). NSAIDs suppress COX activity and have become the major means of relieving chronic pain related to rheumatoid and osteoarthritis. They are also commonly used as analgesics for alleviating serious post-surgical pain. PGs are commonly known to play a serious function in bone healing and natural bone homeostasis. Animal studies mention that both nonspecific and specific COXs inhibitors weaken fracture healing. Some researchers have mentioned that this impairment is because of COX-2 [37].

As previously mentioned, NSAIDS primarily inhibits the cyclooxygenase enzyme, which is mainly responsible for the transformation of phospholipids to several prostaglandins. Disturbance in the production of prostaglandins impacts the kidneys in a variety of ways, involving vasoconstriction that may cause an ischemic acute kidney injury (AKI) in at-risk people. They also weaken salt and water secretion, causing blood pressure and edema, and the other complications involve hyperkalemia, hyponatremia, and chronic kidney disease improvement. Acute kidney injury from NSAIDs is commonly reversible after discontinuation of NSAIDs [38].

1.5 Objectives of the study

The basic target of our study is introducing a chemical variety into the molecular domain to synthesize active molecules with a wide range of structures. After defining the problem, we explain the goals of the thesis in details.

1. This work's overall goal was to synthesize a library of COX-1 and COX-2 inhibitors.

2. One of the major aims of this work was to describe the physical and chemical characteristics of the novel synthesized derivatives.

3. In vitro testing on COX-1 and COX-2 enzyme screening kits.

4. The thesis aims to develop an overarching framework to discover novel compounds with effective inhibitory activities versus COX enzymes.

Chapter Two

Methodology

2.1 Reagents and materials

All chemicals were bought from C.S Chemicals Company, Sigma-Aldrich, and Alfa Aesar and used without additional purification. 2-(3-Methoxyphenyl)-4-methylthiazole-5-carboxylic acid (catalog # H54566), 1-(3-Dimethylaminopropyl)-3-ethylcarbodiimide hydrochloride (EDC) (catalog # A10807), 4-Methylthioaniline (catalog # L04950), 4-(2-Methoxyphenoxy) aniline (catalog # H32565), and 3-(Trifluoromethyl)aniline (catalog # A15910) were bought from Alfa Aesar Company. 4-(Dimethylamino) pyridine (DMAP) (catalog # 39405-50G), 3,4,5-Trimethoxyaniline (catalog # T68209-10G), Sodium sulphate anhydrous, Silica gel (catalog # S74874), 4-Tertbutylaniline (catalog # 209864), 3,4-Dimethoxyaniline (catalog # A83008), 3,5-Dimethoxyaniline (catalog # D130001), Aniline (catalog # 132934), 2,4-Dimethoxyaniline (catalog # D129801-100G), and 2,5-Dimethoxyaniline (catalog # 112984-250G) were bought from Sigma-Aldrich Company. Hcl 32%, COX inhibitor screening assay kit No. 560131 (Cayman Chemical, USA), RPMI 1640 media[-](L-Glutamine), DMEM media, Trypsin EDTA solution B, MTS reagent. L-Glutamine solution and Fetal Bovine Serum Brazil Origin both were bought from Sigma-Aldrich Company.

Acetone, methanol, ethanol, Hexane, dichloromethane (DCM), and Ethyl acetate were bought from C.S Chemicals Company.

2.2 Instruments

Melting points were defined with a GALLENKAMP Melting Point Apparatus, Vacuubrand rotary evaporator complet, Upland UV-lamp, LABOMED Inverted fluorescence microscope, ESCO laminar flow cabinet, BIOBASE medical CO2 Incubator, Lab Tech Digital water bath, J.P. SELECTA digital vortex, and ADAM balance.

To carry out ^{1}H-NMR and ^{13}C-NMR spectra, two NMR instruments were utilized. The first was a Burker 500MHz-Avance III High-Performance Digital FT-NMR spectrometer at the Faculty of Science, University of Jordan, Jordan. The solvent utilized in both instruments was DMSO-d6, and the internal standard was Tetramethyl

sailane. All chemical shifts were recorded as δ (ppm). High-resolution mass spectra data (HRMS) were collected using a water LCT Premier XE Mass spectrometer using the ESI (+) method at Pharmacy Faculty Gazi University Ankara-Turkey. COX inhibitor screening assay kit No. 560131 (Cayman Chemical, USA) was used to determine the inhibitory activity of ovine COX-1 and human recombinant COX-2 enzyme. Utilizing a UV spectrophotometer at a 415nm wavelength and a microplate reader (Bio-Rad Japan), the yellow result of this enzymatic reaction is identified.

2.3 Synthesis and biological evaluation of products

The whole synthetic procedures were conducted at laboratories of An-Najah National University.

2.4 General synthetic procedures

In a clean round, bottom flask 2-(3-Methoxyphenyl)-4-methylthiazole-5-carboxylic acid (300mg, 1.203 mmol) was dissolved in 15ml DCM, then DMAP (45mg, 0.361mmol) was added and stirred under argon gas to prevent oxidation, after 5-10 min EDCI (305.91mg, 1.5639mmol) was added which is a coupling reagent and stirred under the argon gas, then after 30min aniline derivative was added, and the reaction mixture stilled with stirrer for 48hrs. TLC papers one was pigmented with Ninhydrin to detect the presence of aniline. The other one with bromocresol to detect the presence of acid to be sure the product was pure, then washing the reaction mixture with Hcl 32% to separate the aniline derivative by separatory funnel (extraction). The lower layer was leaked inside a conical flask. Sodium sulphate anhydrous (drying agent) was added to the flask and filtered by filter paper (filtration step). Silica gel was added (3-4 spatulas) to the filtrate then vacuum evaporation was used to remove the reaction mixture by a rotary vacuum evaporator considering the DCM boiling point of 39.6 °C to have a product loaded silica in the flask. The product-loaded silica was purified by silica gel column chromatography using a DCM:Ethyl acetate (1:1) solvent system, and tubes containing the product were collected and then evaporated.

2.4.1 Synthesis of 2-(3-methoxyphenyl)-4-methyl-N-(3,4,5-trimethoxyphenyl) thiazole-5-carboxamide (2a)

Same as the previous procedure, and the aniline derivative used here was 3,4,5-trimethoxy aniline (249.86mg,1.323mmol)

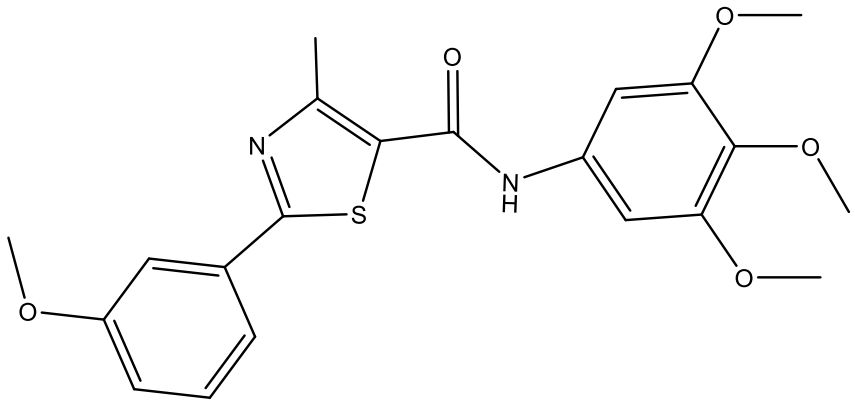

White powder product with **R_f**:0.71 (DCM: EtOAc 1:1). The percentage yield is 66%.

HRMS (m/z): $[M+H]^+$ calcd. for $C_{21}H_{22}N_2O_5S$ 415.1240, found 415.1252

^{1}H-NMR (DMSO-d_6, 500 MHz) δ ppm: 10.16 (1H, s, N-H), 7.55 (1H, d, J = 7.5 Hz, Ar-H), 7.49-7.12 (5H, m, Ar-H), 3.86 (3H, s, O-CH3), 3.77 (6H, s, O-CH3), 3.65 (3H, s, O-CH_3), 2.66 (3H, s, -CH_3).

^{13}C-NMR (DMSO-d_6, 125 MHz) δ ppm: 166.42, 160.25, 160.05, 156.39, 153.11, 135.20, 134.46, 134.10, 131.10, 126.52, 119.24, 117.48, 111.30, 98.57, 60.58, 56.22, 55.82, 17.63. See Appendix A for the spectrum.

2.4.2 Synthesis of N-(4-(tert-butyl) phenyl)-2-(3-methoxyphenyl)-4-methylthiazole-5-carboxamide (compound 2b)

Here the aniline derivative was 4-tert-butylaniline (212.88mg,1.323mmol), and the product-loaded silica was purified by silica gel column chromatography by using Hexane:Ethyl acetate (3:2) solvent system.

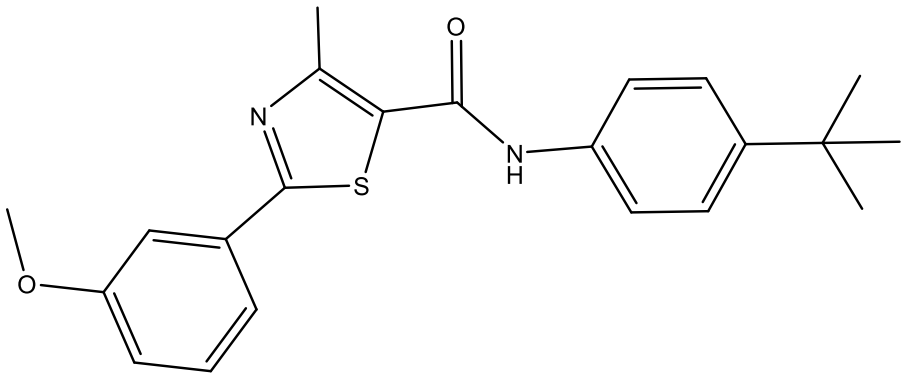

Beige crystals product with R_f:0.6 (Hex: EtOAc 3:2). The percentage yield is 50%.

HRMS (m/z): $[M+H]^+$ calcd. for $C_{22}H_{24}N_2O_2S$ 383.1320, found 381.1313

^{1}H-NMR (DMSO-d_6, 500 MHz) δ ppm: 10.20 (1H, s, N-H), 7.61 (2H, d, J = 7 Hz, Ar-H), 7.55 (1H, d, J = 7.5 Hz, Ar-H), 7.49 (1H, s, Ar-H), 7.46 (1H, t, J = 8 Hz, Ar-H), 7.38 (2H, d, J = 7 Hz, Ar-H), 7.12 (1H, d, J = 8 Hz, Ar-H), 3.86 (3H, s, O-CH_3), 2.66 (3H, s, -CH_3), 1.29 (9H, s, t-butyl).

^{13}C-NMR (DMSO-d_6, 125 MHz) δ ppm: 166.40, 160.25, 160.07, 155.96, 146.90, 136.50, 134.14, 131.09, 126.90, 125.79, 120.62, 119.25, 117.46, 111.30, 55.83, 34.56, 31.64, 17.58. See Appendix A for the spectrum.

2.4.3 Synthesis of N-(3,4-dimethoxyphenyl)-2-(3-methoxyphenyl)-4-methylthiazole-5-carboxamide (compound 2c)

Aniline derivative was 3,4-dimethoxy aniline (206.839 mg,1.323 mmol).

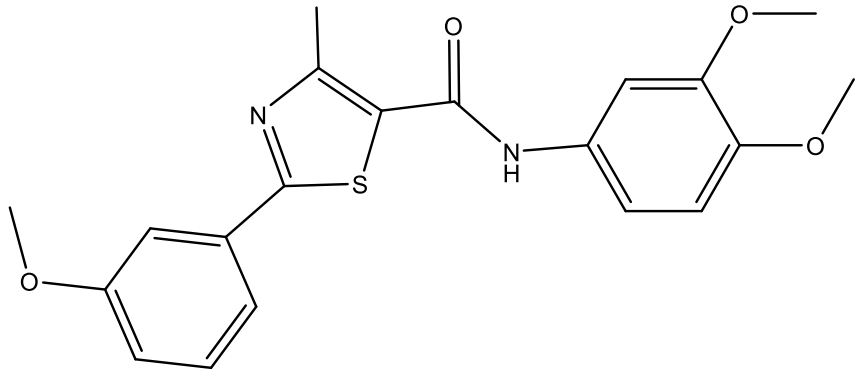

Soft gray powder product with R_f:0.74 (DCM: EtOAc 1:1). The percentage yield is 44%.

HRMS (m/z): $[M+H]^+$ calcd. for $C_{20}H_{20}N_2O_4S$, 385.1085, found 385.1099.

^{1}H-NMR (DMSO-d_6, 500 MHz) δ ppm: 10.10 (1H, s, N-H), 7.55 (1H, d, J = 7.5 Hz, Ar-H), 7.49-7.44 (2H, m, Ar-H), 7.38 (1H, s, Ar-H), 7.25 (1H, d, J = 8.5 Hz, Ar-H), 7.12 (1H, d, J = 8 Hz, Ar-H), 6.94 (1H, d, J = 8.5 Hz, Ar-H), 3.86 (3H, s, O-CH3), 3.76, 3.75 (6H, s, OCH3), 2.66 (3H, s, -CH3).

^{13}C-NMR (DMSO-d_6, 125 MHz) δ ppm: 166.28, 160.24, 159.85, 156.03, 148.93, 145.92, 134.14, 132.55, 131.09, 126.77, 119.23, 117.45, 112.91, 112.33, 111.29, 105.97, 56.17, 55.88, 55.82, 17.58. See Appendix A for the spectrum.

2.4.4 Synthesis of N-(3,5-dimethoxyphenyl)-2-(3-methoxyphenyl)-4-methylthiazole-5-carboxamide (compound 2d)

3,5-dimethoxy aniline was the aniline derivative (206.839mg,1.323 mmol).

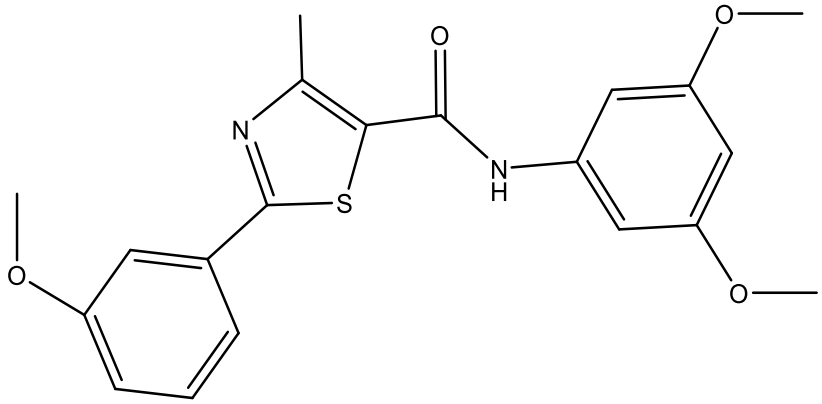

White crystals product with R_f:0.74 (DCM: EtOAc 1:1). The percentage yield is 56%.

HRMS (m/z): $[M+H]^+$ calcd. for $C_{20}H_{20}N_2O_4S$, 385.1085, found 385.0765

^{1}H-NMR (DMSO-d_6, 500 MHz) δ ppm: 10.19 (1H, s, N-H), 7.55 (1H, d, J = 7.5 Hz, Ar-H), 7.49-7.44 (2H, m, Ar-H), 7.12 (1H, d, J = 7.5 Hz, Ar-H), 6.99 (2H, s, Ar-H), 6.30 (1H, s, Ar-H), 3.86 (3H, s, O-CH3), 3.74 (6H, s, OCH3), 2.65 (3H, s, -CH3).

^{13}C-NMR (DMSO-d_6, 125 MHz) δ ppm: 166.52, 160.88, 160.25, 156.32, 140.76, 134.09, 131.10, 126.63, 119.25, 117.50, 111.31, 98.99, 96.52, 55.83, 55.61, 17.61. See Appendix A for the spectrum.

2.4.5 Synthesis of 2-(3-methoxyphenyl)-4-methyl-N-(4-(methylthio)phenyl)thiazole-5-carboxamide (compound 2e)

4-(methylthio) aniline (167.859 µL,1.323 mmole) was used. There was no need for adding silica and purifying by silica gel column chromatography because TLC showed that the product was pure.

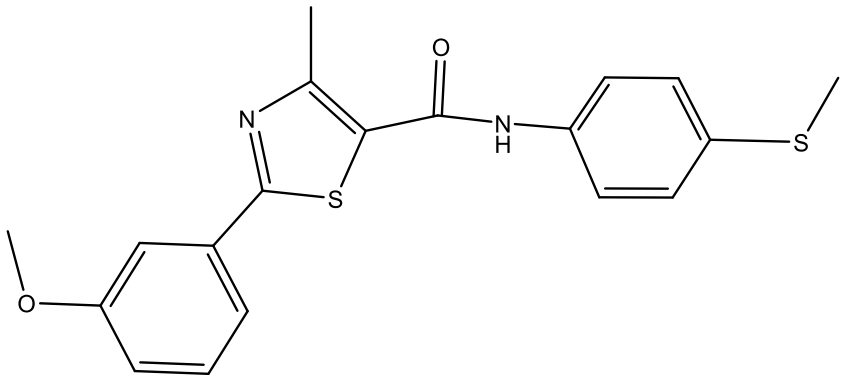

Coarse dark green powder product with R_f:0.75 (DCM: EtOAc 1:1). The percentage yield is 65.5%.

HRMS (m/z): $[M+H]^+$ calcd. for $C_{19}H_{18}N_2O_2S_2$, 371.0515, found 371.0508

^{1}H-NMR (DMSO-d_6, 500MHz) δ ppm: 10.29 (1H, s, N-H), 7.67 (2H, d, J = 8 Hz, Ar-H), 7.55 (1H, d, J = 7.5 Hz, Ar-H), 7.49-7.44 (2H, m, Ar-H), 7.28 (2H, d, J = 8 Hz, Ar-H), 7.12 (1H, d, J = 8 Hz, Ar-H), 3.85 (3H, s, O-CH3), 2.66 (3H, s, -CH3), 2.47 (3H, s, S-CH3).

^{13}C-NMR (DMSO-d_6, 125 MHz) δ ppm: 166.49, 160.24, 160.11, 156.21, 136.49, 134.10, 133.36, 131.09, 127.29, 126.66, 121.49, 119.25, 117.48, 111.31, 55.83, 17.62, 15.83. See Appendix A for the spectrum**.**

2.4.6 Synthesis of 2-(3-methoxyphenyl)-4-methyl-N-phenylthiazole-5-carboxamide (compound 2f)

Photosensitive aniline (123.288 μL, 1.323 mmol), there was no need for purifying by silica gel column chromatography.

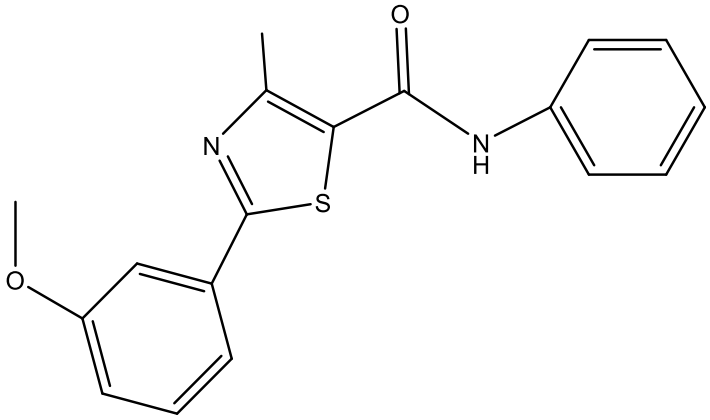

Coarse Beige powder product with R_f: 0.62 (DCM: EtOAc 1:1). The percentage yield is 57.1%.

HRMS (m/z): $[M+H]^+$ calcd. for $C_{18}H_{16}N_2O_2S$, 325.0555, found 325.0545.

^{1}H-NMR (DMSO-d_6, 500 MHz) δ ppm: 10.26 (1H, s, N-H), 7.70 (2H, d, J = 8 Hz, Ar-H), 7.55 (1H, d, J = 7.5 Hz, Ar-H), 7.50-7.44 (2H, m, Ar-H), 7.37 (2H, t, J = 7.5 Hz, Ar-H), 7.15-7.11 (2H, m, Ar-H), 3.86 (3H, s, O-CH3), 2.66 (3H, s, -CH3).

^{13}C-NMR (DMSO-d_6, 125 MHz) δ ppm: 166.50, 160.31, 160.24, 156.12, 139.06, 134.11, 131.10, 129.17, 126.78, 124.53, 120.85, 119.26, 117.47, 111.32, 55.83, 17.59. See Appendix A for the spectrum.

2.4.7 Synthesis of N-(2,4-dimethoxyphenyl)-2-(4-methoxyphenyl)-4-methylthiazole-5-carboxamide (compound 2g)

Photosensitive 2,4-dimethoxy aniline (194.392 μL,1.323 mmol) was used, it was no need for purifying by silica gel.

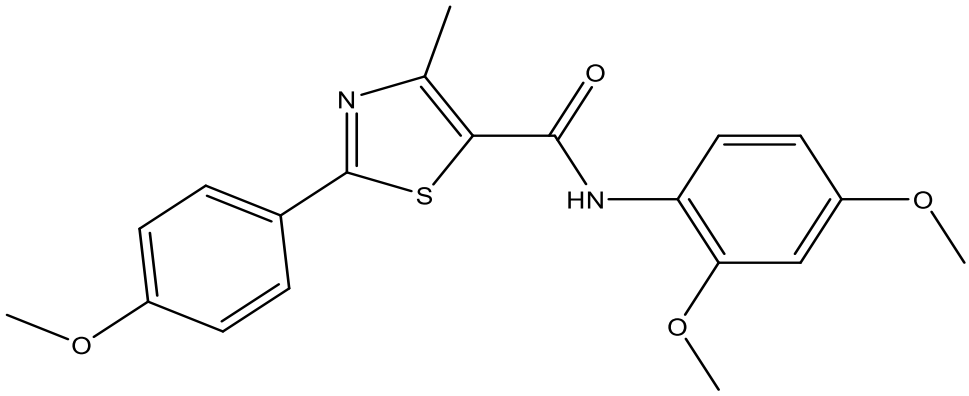

Soft green powder product with R_f:0.72 (DCM: EtOAc 1:1). The percentage yield is 61%.

HRMS (m/z): $[M+H]^+$ calcd. for $C_{20}H_{20}N_2O_4S$, 385.1085, found 385.1178

^{1}H-NMR (DMSO-d_6, 500 MHz) δ ppm: 9.22 (1H, s, N-H), 7.56 (1H, d, J = 8 Hz, Ar-H), 7.53 (1H, d, J = 7.5 Hz, Ar-H), 7.48-7.43 (2H, m, Ar-H), 7.11 (1H, d, J = 8 Hz, Ar-H), 6.68 (1H, s, Ar-H), 6.55 (1H, d, J = 8.5 Hz, Ar-H), 3.85, 3.83, 3.78 (9H, s, O-CH_3), 2.69 (3H, s, -CH_3).

^{13}C-NMR (DMSO-d_6, 125 MHz) δ ppm: 166.51, 160.31, 160.22, 158.44, 155.38, 153.44, 134.17, 131.04, 125.93, 119.89, 119.29, 117.38, 111.32, 104.71, 99.44, 97.33, 56.34, 55.83, 55.81, 17.62. See Appendix A for the spectrum.

2.4.8 Synthesis of N-(2,5-dimethoxyphenyl)-2-(3-methoxyphenyl)-4-methylthiazole-5-carboxamide (compound 2h)

Photosensitive 2,5-dimethoxy aniline (206.79 mg,1.323 mmol) was used.

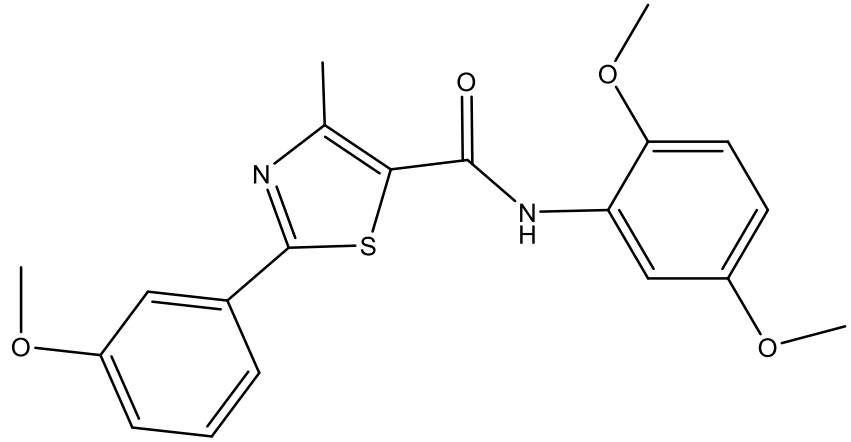

Soft gray powder product with R_f:0.50 (DCM: EtOAc 1:1). The percentage yield is 40%.

HRMS (m/z): $[M+H]^+$ calcd. for $C_{20}H_{20}N_2O_4S$, 385.1085, found 385.1205

^{1}H-NMR (DMSO-d_6, 500 MHz) δ ppm: 9.21 (1H, s, N-H), 7.60 (1H, s, Ar-H), 7.55 (1H, d, J = 7.5 Hz, Ar-H), 7.49-7.44 (2H, m, Ar-H), 7.12 (1H, d, J = 8.5 Hz, Ar-H), 7.04 (1H, d, J = 9 Hz, Ar-H), 6.75 (1H, d, J = 9 Hz, Ar-H), 3.86, 3.83, 3.73 (9H, s, O-CH_3), 2.72 (3H, s, -CH_3).

^{13}C-NMR (DMSO-d_6, 125 MHz) δ ppm: 166.92, 160.23, 159.86, 155.49, 153.41, 145.08, 134.07, 131.06, 127.81, 127.77, 119.35, 117.50, 112.64, 111.38, 110.00, 109.60, 56.92, 55.91, 55.84, 17.71. See Appendix A for the spectrum.

2.4.9 Synthesis of N-(4-(2-methoxyphenoxy)phenyl)-2-(3-methoxyphenyl)-4-methylthiazole-5-carboxamide (compound 2i)

4-(2-methoxyphenoxy) aniline (293.58 mg,1.323 mmol) was the aniline derivative.

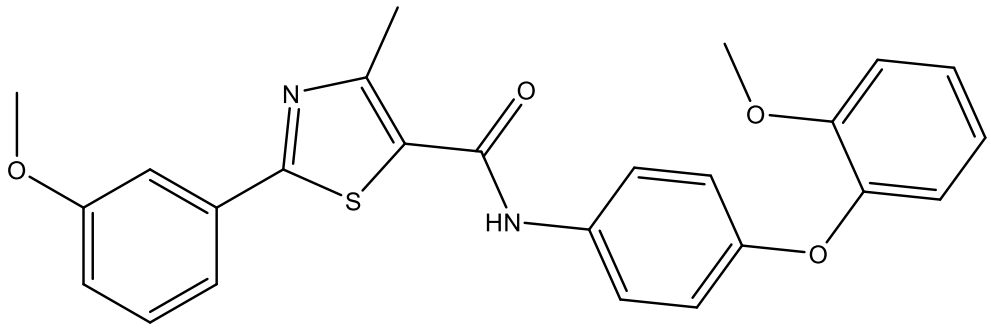

Soft white powder product with R_f:0.78 (DCM: EtOAc 1:1). The percentage yield is 65.2%.

HRMS (m/z): $[M+H]^+$ calcd. for $C_{25}H_{22}N_2O_4S$, 447.1390, found 447.1373

^{1}H-NMR (DMSO-d_6, 500 MHz) δ ppm: 10.20 (1H, s, N-H), 7.62 (2H, d, J = 8 Hz, Ar-H), 7.55 (1H, d, J = 7.5 Hz, Ar-H), 7.49-7.44 (2H, m, Ar-H), 7.21-7.16 (2H, m, Ar-H), 7.12 (1H, d, J = 8 Hz, Ar-H), 7.03 (1H, d, J = 8 Hz, Ar-H), 6.99 (1H, t, J = 7 Hz, Ar-H), 6.86 (2H, d, J = 8 Hz, Ar-H), 3.85, 3.76 (6H, s, O-CH_3), 2.65 (3H, s, -CH_3).

^{13}C-NMR (DMSO-d_6, 125 MHz) δ ppm: 166.40, 160.24, 160.00, 156.04, 154.56, 151.69, 144.42, 134.13, 133.57, 131.09, 126.74, 125.81, 122.60, 121.68, 121.55, 119.24, 117.45, 116.88, 113.87, 111.31, 56.08, 55.82, 17.58. See Appendix A for the spectrum**.**

2.4.10 Synthesis of 2-(3-methoxyphenyl)-4-methyl-N-(3-(trifluoromethyl) phenyl) thiazole-5-carboxamide (compound 2j)

3-(Trifluoromethyl) aniline (166.3 μL,1.323 mmol).

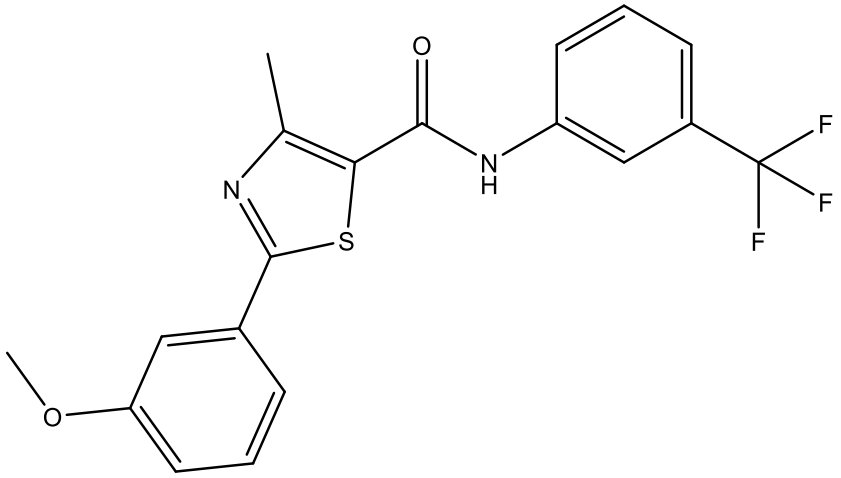

Coarse white powder product with R_f:0.65(DCM: EtOAc 1:1). The percentage yield is 86.3%.

HRMS (m/z): $[M+H]^+$ calcd. for $C_{19}H_{15}F_3N_2O_2S$, 393.0780, found 393.0772

^{1}H-NMR (DMSO-d_6, 500 MHz) δ ppm: 10.56 (1H, s, N-H), 8.17 (1H, s, Ar-H), 7.96 (1H, d, J = 8 Hz, Ar-H), 7.62 (1H, d, J = 7.5 Hz, Ar-H), 7.56 (1H, d, J = 7.5 Hz, Ar-H), 7.50-7.45 (3H, m, Ar-H), 7.13 (1H, d, J = 7.5 Hz, Ar-H), 3.86 (3H, s, O-CH_3), 2.68 (3H, s, -CH_3).

^{13}C-NMR (DMSO-d_6, 125 MHz) δ ppm: 166.89, 160.64, 160.26, 157.07, 139.88, 134.02, 131.13, 130.45, 130.01, 129.76, 125.99, 124.38, 120.83, 119.29, 117.60, 116.94, 111.36, 55.83, 17.70. See Appendix A for the spectrum**.**

2.5 General procedure of performing column chromatography

A proper column size was selected, and the column was prepared by adding silica gel to the cotton-capped column and then adding the product-loaded silica. Five layers were added to the cotton-capped column, sand, silica gel, sand, product-loaded silica, and sand, as shown in figure 2. Dissolving the product was by mobile gradient phase, which TLC optimized. Finally, tubes were collected after elution for analysis.

2.6 Cell culture and cytotoxicity assay

Common cell line (Hek293T) and human hepatic stellate (LX-2) were grown in RPMI-1640 media with 1% penicillin/streptomycin antibiotics, 10% fetal bovine serum, and 1% l-glutamine.

In general, carefully perfusion of the culture media from the culture vessel without causing a cell monolayer defect, and the culture flask was gently tilted**.** Aspirating DPBS from the culture flask without causing a defect on the cell monolayer, 1 ml Trypsin was added, gently tilted, and incubated at 37c for 5 min. When the majority of cells have separated, 10 ml corresponding culture media is added, and gently vortex or pipette the culture suspension to guarantee the neutralization is complete. Gently pipettes the cells up and down 4-6 times till reaching a similar distribution, then 10 µl of cell suspension was added between the hemocytometer and cover glass. Counting the number of cells in all four outer squares,$1x10^4$ cell /ml ($1x10^3$ cell /100µl) needed and 100µl / well were added (96 well plate was used) and then incubated at 37 ◦C for 24 h.

24 hours later, the media was removed carefully to avoid disturbing the cell. With the addition of 100 µl/well of different drug concentrations, which is prepared before then Incubation72 h at 37 ◦C, the drug was removed without causing a disturbance in the cell to stop the effect of the drug on absorbance, in accordance with manufacturer's recommendations, the Cell Tilter 96® aqueous one solution cell proliferation (MTS) test evaluated the viability of the cells (Promega Corporation, Madison, WI). 20 µl of MTS solution was added and incubated for 2 h, then reading the absorbance by ELISA reader at 49 nm and IC_{50} was calculated.

The freezer temperature was -20 °C.

2.7 Biological assay on COX enzyme screening kits

The inhibitory impact of arachidonic acid PGH2 conversion by human recombinant COX-2 and bovine COX-1 was estimated using the COX (human) Inhibitor Screening Test Kit (provided by Cayman chemicals assay kit No. 560131).

The synthesized product has a similar structure to Celecoxib, so as a positive control in the test, celecoxib was employed..

Testing method and reagents prepared as the manufacturer recommended. Two concentrations of the inhibitors and celecoxib (40 and 5 µM) were dissolved in dimethyl sulfoxide (DMSO) and then incubated for 10 min at 37 ℃ with a mixture of COX-1 or COX-2 enzyme. Related to the heme was in the diluted reaction buffer. Initiated the reaction by adding 10 µl of arachidonic acid and incubating for thirty seconds at 37 ℃. 30 µl stannous chloride was inserted to stop the enzyme catalysis, followed by incubation for five minutes at room temperature.

Quantification by ELISA was performed on produced prostaglandins. On an orbital shaker, the 96 –well plates were wrapped in a plastic film and then incubated for 18 h at room temperature. After that, the plate was washed five times by using a wash buffer after emptying of wells, then 200µl of Ellman's reagent was added to each well and 5 µl of tracer to the TA wells. The plate was incubated in the dark plate for 60-90 min at room temperature until the absorbance of the B0 and in the 0.3-0.8 range at 405 nm.

Unilab microplate reader 6000 was used for reading the plate. IC_{50} was calculated from the curve of the inhibitory response to concentration. To calculate the selectivity index (SI), the IC50 COX-1 and COX-2 were divided [39].

2.8 3-Methoxy phenyl 4-methyl-thiazole derivatives as COX inhibitors

2.8.1 Molecular Docking Studies

Out of the 10 newly designed molecules, the ligands A, B, and J, which displayed the most potency and highest Selectivity Index (SI) values toward the COX-2 isoform, were selected for docking studies. Starting with building the 3-D structures and preparing the selected ligands to be convenient for docking studies, the build panel integrated into maestro-Schrödinger 12.1 was utilized, followed by subjecting to *Ligprep* module for preparation which involves: realistic bond angles and bond length, the addition of

hydrogens, and generates ionization states at target pH (7.0 ± 2.0) protonation state, stereo chemistries and ring conformations, tautomers, low energy structures, and corrected chiralities. Then, the generated geometries of prepared ligands were minimized at the optimized potential for liquid simulations (OPLS-2005) force field using a default setting until getting an RMSD cut of 0.001 Å. The final minimized structures were then saved for docking studies.

Both crystallized human cyclooxygenase enzymes COX-1 (PDB ID: 3KK6) and COX-2 (PDB ID: 5KIR) complexed with celecoxib and rofecoxib, respectively, were downloaded from Protein Data Bank[40]. These two crystal structures were evaluated properly in previous studies and displayed relevant binding orientations[27]. By use of the Protein Preparation Wizard already incorporated in the maestro program, the obtained PDB complex structures were optimized chemically and structurally[41]. Also, the protein preparation tool aims to add the H-atoms to the receptor structures, remove water molecules beyond 5 Å from the hit group, and assign bonding orders and charges. Then, the prepared protein structures were reduced using the OPLS_2005 force field with a root mean square deviation (RMSD) value of 0.30 Å. To define the active site docking studies, The Maestro Receptor Grid Generation tool was used to create the receptor grids, and the default parameters were kept. At last, to conduct molecular docking experiments, the finally prepared ligands and generated receptor grids were exported to the Glide module integrated into Maestro- Schrödinger molecular modeling software, and the extra-precision Glide docking mode was employed [42, 43]. The docked position with the lowest docking score (Glide score) out of all those created for each ligand was kept as the best pose and saved for each ligand. To precisely investigate the binding interactions within the binding pocket, ultimately chosen docked postures were exported to Protein-Ligand Interaction Profiler (PLIP) server and visualized using PyMol 2.5.2 software[44, 45].

2.8.2 Free energy calculations using Prime MM-GBSA

To evaluate the ligand strain energies and the ligand binding energies regarding the selected docked molecules inside the location where COX-1 and COX-2 receptors bind, the Prime Molecular mechanics – Generalized Born Model and Solvent accessibility (Prime MM-GBSA) model was used, which is integrated into the Maestro-Schrödinger 12.1 program. The Prime MM-GBSA model worked at VSGB solvent model and

OPLS-2005 force field[46]. Thus, the total free energy of ligand-receptor binding was calculated using the resulting viewer file for the docked ligands' glide positions. Upon binding, the following equation is applied to calculate the changes in free energy:

$$\Delta G_{bind} = G_{complex} - (G_{protein} + G_{ligand} \quad \text{Eq.2}$$

Where ΔG_{bind} is the ligand-binding energy, $G_{complex}$, $G_{protein}$, and G_{ligand} are, respectively, the minimized energies of the protein-ligand complex, the unbound protein, and the unbound ligand.

2.8.3 Density Functional Theory Analysis

The obtained conformations of selected ligands (A, B, and J) and celecoxib were exported to the Jaguar module (Schrödinger) to perform DFT calculations. Subsequently, a group of global reactivity descriptors could be defined as Lowest Unoccupied Molecular Orbital (E_{LUMO}), Highest Occupied Molecular Orbitals (E_{HOMO}), HOMO-LUMO gap (ΔE), and atomic electrostatic potential charges (ESP) [47, 48]. Using DFT, the geometries of selected ligands were properly optimized involves the use of the basis set of 6-31G** and the Becke three-parameter exchange potential and yang-Parr correlation functional (B3LYP) [49-51].

The HOMO orbital with elevated energy values is always directly related with an electrophilic attack due to the strong ability to donate electrons. Otherwise, the high probability of LUMO orbitals accepting electrons makes its straightforward correlation with a nucleophilic attack [52, 53]. The distinction in energies between HOMO and LUMO is the electronic excitation energy named the HOMO-LUMO gap (ΔE) energy which is a descriptor applied to assess the molecular reactivity and stability[54, 55]. By decreasing the ΔE value, the molecule's global hardness decreases, indicating the molecule's high reactivity but concomitantly, with low stability [56].

The electrostatic potential map surfaces of the selected ligand were also constituted using DFT calculations within the Jaguar module to specify the electron-rich regions and electron-poor concentrate regions.

2.8.4 Drug Likeness Analysis

The drug-likeness of all our recently developed compounds was evaluated by calculating a set of descriptors related to ADME-T. This set of ADME-T parameters was determined to ensure that the newly designed ligands agree with the potential drug candidates with respect to physicochemical and pharmacokinetic parameters. The ADME-T descriptors were determined utilizing the QikProp module of the Schrödinger suite (Schrödinger Release 2021-4). It is easy to use, quick, and accurate [57].

Chapter Three

Results and Discussion

3.1 Chemistry

According to Scheme 1, thiazole carboxamide derivatives (2a–2j) were created. The 2-(3-methoxyphenyl)-4-methylthiazole-5-carboxylic acid was dissolved in DCM, and then DMAP and EDCI were added and mixed under argon gas to create the 2-(3-methoxyphenyl)-4-methyl-N-(3,4,5-trimethoxyphenyl) thiazole -5-carboxamide compound 2a. 3,4,5-trimethoxy aniline was added after 30 minutes, and the reaction was stirred for 48 hours before being extracted with Hcl 32%, sodium sulphate anhydrous, and filtration was done. Except for the 2e, 2f, 2g, 2h, and 2j compounds, most of the produced products were purified using column chromatography.

Scheme 1

After stirring 1 + Aniline derivatives in 20 ml of DCM for 48–72 hours, the addition of DMAP and EDC while argon gas was present.

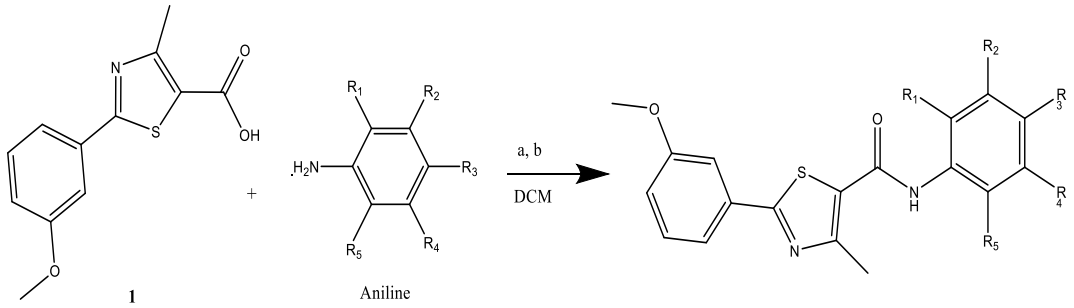

2a R2=OCH3, R3=OCH3, R4=OCH3
2b R3=C(CH3)3
2c R2=OCH3, R3=OCH3
2d R2=OCH3, R4=OCH3
2e R3=SCH3
2f -
2g R3=OCH3, R5=OCH3
2h R1=OCH3, R4=OCH3
2i R3=

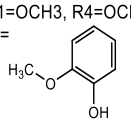

2j R4=CF3

3.2 In vitro evaluation of cytotoxicity

LX-2 (normal liver) and Hek293t (normal kidney) were used in the MTS assay to define the cytotoxic effect of thiazole carboxamide derivatives. This test used five different concentrations (300, 100, 50, 10, and 1 µM).

All compounds exhibited negligible cytotoxic activity versus the evaluated normal cell lines. The IC_{50} values were more than 300 µM, except compound **2b** IC_{50} values were 203.71±1.89 and 116.96±2.05 µM against LX-2 and Hek293t cell lines, respectively. The inhibition percentage of all of these compounds were presented in figures 3.1 and 3.2 compared to the positive control 5-FU.

Figure 3.1

Inhibition percentage of all compounds compared to the positive control 5-FU by using LX-2 cells

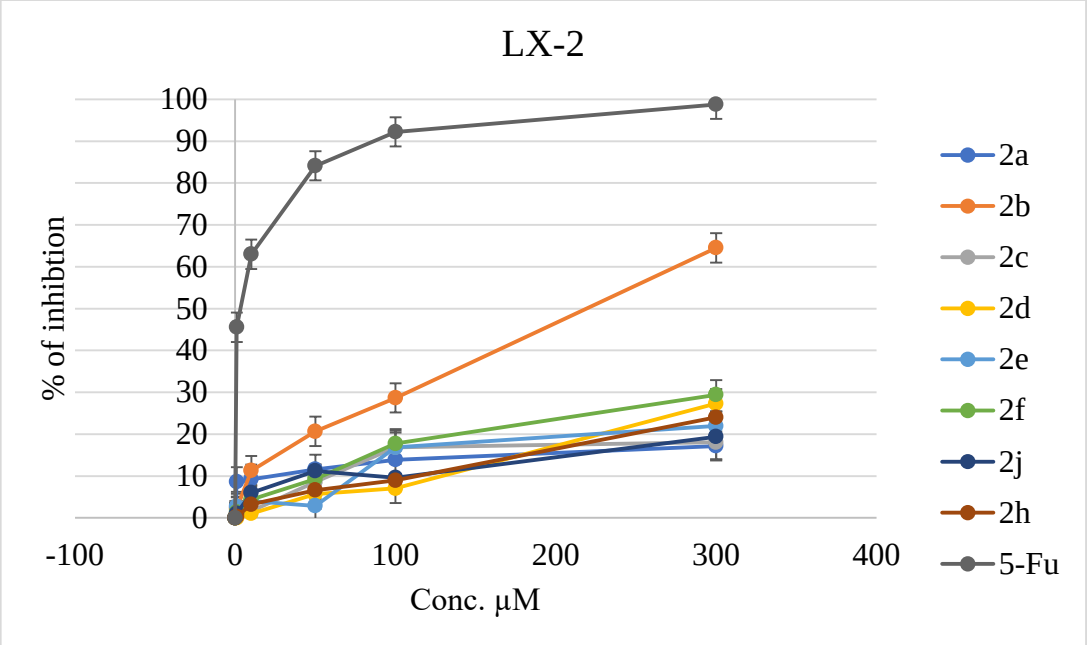

Figure 3.2

Inhibition percentage of all compounds compared to the positive control 5-FU by using Hek293t cells

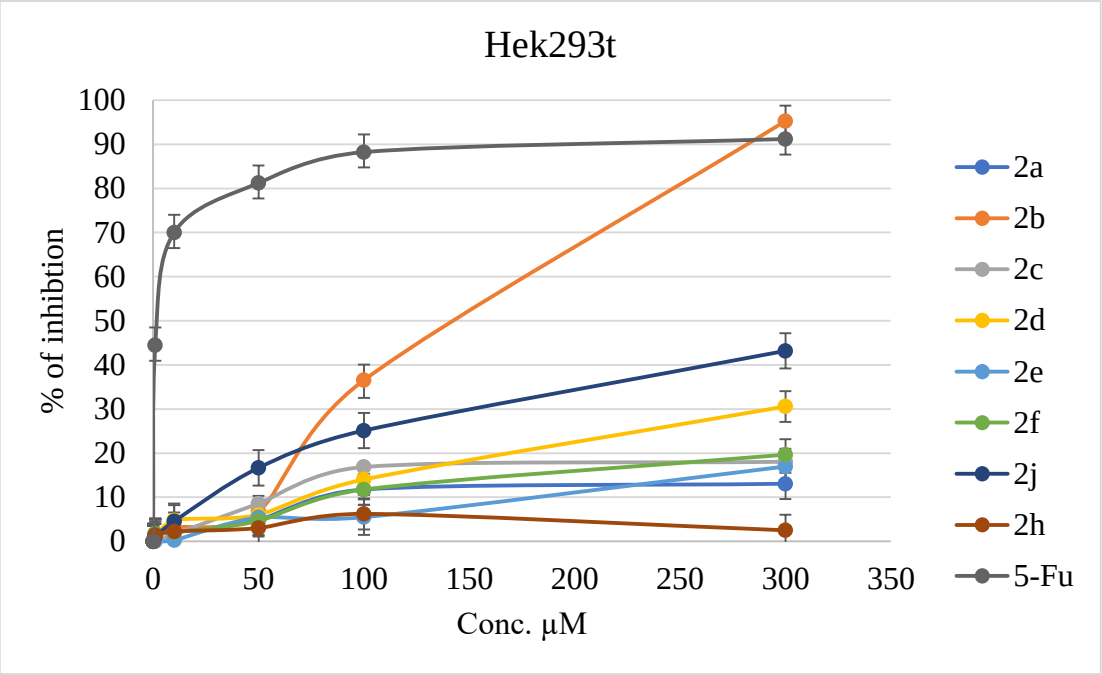

3.3 3-methoxy phenyl 4-methyl-thiazole derivatives as COX inhibitors

Celecoxib was used as a positive control, and two serial concentrations were tested (40 and 5 µM). The selectivity (SI) and 50% of the maximum inhibitory level (IC50) were computed, shown in Table **2,** for synthesized compounds.

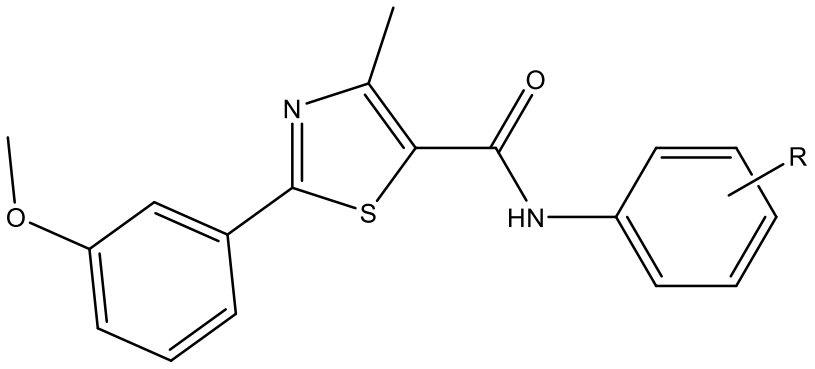

Table 2

half-maximal inhibitory concentration (IC_{50}) and selectivity index (SI) for thiazole carboxamide derivatives compounds

			IC_{50} (µM)			CC_{50} (µM)	
original code	new code	R	COX1	COX2	SI	Hek293t	LX-2
RS1	2a	3,4,5-triemthoxyphenyl	2.65	0.958	2.76618	>300	>300
RS2	2b	4-t-butyl	0.2393	0.1912	1.251569	116.963	203.716
RS3	2c	3,4-dimethoxy	0.2786	2.9057	0.095881	>300	>300
RS4	2d	3,5-dimethoxy	1.5749	2.298	0.685335	>300	>300
RS6	2e	4-S-CH3	1.531	2.117	0.723193	>300	>300
RS7	2f	H	2.055	3.258	0.630755	>300	>300
RS8	2g	2,4-dimethoxy	0.6317	1.803	0.350361	>300	>300
RS9	2h	2,5-dimethoxy	0.335	1.228	0.272801	>300	>300
RS10	2i	4-(2-methoxyphenoxy)	2.111	3.239	0.651744	>300	>300
RS11	2j	3-CF3	1.443	0.957	1.507837	>300	>300
+Ve con			[a]0.0476	[a] 0.002	[a] 23.8	[b] 4.058	[b] 8.45

Note: *P*-value ≤ 0.05; positive controls: [a] Celecoxib, [b] 5-FU

See Appendix B for the spectrum.

Standard deviation (σ) for IC_{50} COX-1 = 0.8211

Standard deviation (σ) for IC_{50} COX-2 = 1

The most effective synthetic drug against the COX-1 enzyme had an IC_{50} value of 0.2393 µM, and it also displayed strong activity on the COX-2 enzyme with an IC_{50} value of 0.1912 µM and a selectivity ratio (1.2515). The highest selectivity ratio was (2.7661) for 2a compound against COX-2 with IC_{50} = 0.958 relating to celecoxib ratio (23.8), and its IC_{50} against COX-2 =0.002, 2j compound also showed a good selectivity towards COX-2 (1.507) with IC_{50} = 0.957.

Due to oxygen's higher electronegativity than carbon, methoxy substituents on aromatic compounds are often utilized in electrophilic aromatic substitution processes. The negative charge of ortho and para positions caused these locations to be more vulnerable to electrophilic substitution, it is an activating group because it gives the benzene ring a negative charge [58]. 2a compound showed the highest selectivity ratio against COX-2 enzyme and methoxy were R2, R3, and R4 at meta, para, and meta positions (m, p, and m), but other compounds which have a methoxy substituents (2c, 2d, 2g, and 2h) didn't show this activity, such as 2d compound which has a mthoxy at meta positions (R2 and R4) and 2h compound at ortho and meta positions (R1 and R4).

2b compound demonstrated a good potency towards COX-1 and COX-2, despite the straightforward bulky structure, *t*-butyl group has special properties that alter or boost specificity or function as a steric barrier that boosts the stability of compounds containing chemically or enzymatically sensitive groups [59]. 2j compound was potent on COX-2, because Florine is a highly electronegative element with a high propensity to attract shared pair of electrons towards itself, one of the strongest electron-withdrawing groups in structural organic chemistry is the trifluoromethyl (-CF3) group, which typically exhibits this feature by boosting the reactivities of neighboring acidic or electrophilic functional groups[60]. Regarding methylthio group in 2e compound, it's an Electron-donating substituent.

3.3.1 Molecular Docking Studies

To investigate the pattern of ligand-protein binding and orientations within the binding site of COX-1 and COX-2 isozymes, so explaining the COX-2 selectivity over the COX-1 recorded for celecoxib, A, B, and J-molecules, molecular docking studies have been performed. However, the amino acid sequence identity of both isoforms is equal to 67%, replacing the ILE-523 amino acid accommodated inside the binding site of COX-1 with the amino acid VAL-523 in COX-2, resulted in the opening of a new secondary binding pocket. This led to uncovering of the new polar amino acid ARG-513, which could involve many polar interactions within the binding site of COX-2. Thus, interacting with ARG-513 is considered an ameliorating COX-2 selectivity.

For each ligand, thirty different orientations were retained from docking simulations. The orientation of each ligand which revealed the lowest binding Glide docking score within the enzyme's binding pocket, was selected as the best to be discussed. **Table 3** summarizes all docking scores of the docked ligands inside COX-1 and COX-2 enzymes. The docking simulations of celecoxib, A, B, and J molecules inside COX-1 and COX-2's enzymes binding location are shown, respectively, in Figures 3.3 and 3.4. Examining the binding pattern of celecoxib as an ideal COX-2 selective (selectivity index (SI) = 23.8) drug over COX-1 showed the optimal occupying and interaction pattern within the COX-2 binding site (Figure 3.4-a), which involves filling the new generated secondary binding pocking and interacting with ARG-513, which are critical interactions for COX-2 selectivity. This additional occupied space and interactions diminished IC_{50} from 47 nM in COX-1 to just 2 nM in COX-2. The absence of this secondary binding pocket in COX1 (Figure 3.3-a) results in rotating the sulfonamide group toward SER-516. Thus the 4-methyl phenyl group generates some steric clashes with the larger amino acid ILE-523 inside COX-1 than VAL-523 presents in COX-2. Other favorable interactions like hydrogen bonds, hydrophobic interactions, and pi-cation interactions also support the significant inhibition activity of celecoxib in the COX-2 enzyme.

Examining the interaction and docking simulation pattern of the B-molecule, which displayed the most COX-2 inhibition activity (IC_{50}= 0.19 μM) in comparison to other newly designed molecules, showed its capability to fill the COX-2 binding site optimally, encompassing the available secondary polar binding pocket. A large

substituent like a t-butyl group pushed the Meta-methoxy phenyl fragment to step inside this secondary binding pocket, forming the critical and ameliorating hydrogen bond with ARG-513. Analyzing the docking simulation of B-molecule using PLIP software indicated the formation of additional hydrogen bonds with TYR-385 and SER-530 and 13 water-repellent interactions between the nearby amino acids like VAL-116, PHE-518, ILE-517, and LEU-531(Figure 3.4-c). The high inhibition activity of B-molecule recorded against COX-1 isozyme (IC_{50}=0.239 μM) could be explained via forming 6 favorable hydrogen bonds with TYR-355, HIS-90, ARG-120, GLN-192, SER-353, and SER-516 (Figure 3.3-c). Also, the *t*-butyl group serves a crucial function in stabilizing B-Molecule in a good geometry within the COX-1 binding pocket by filling the available lipophilic space and forming hydrophobic interactions with the close amino acids like THR-94.

The molecular docking studies of A-molecule in figures 3.3-b and 3.4-b, the binding sites for COX-1 and COX-2, respectively, are shown. The extended conformation of A-molecule and 4,5,6-tri-methoxy substituents show low congruency with the dimensions of the COX-1 binding site. Thus, the three methoxy substituents do not locate within the binding distances, so pay steric and electronic penalties to decrease the COX-1 inhibition potency (IC50= 2.65 μM). A-molecule shows similar interaction patterns within the binding site of COX-2 (creates hydrogen bonds with ARG-120, TYR-355 and Pi-cation bond with TYR-355), but the 3,4,5 tri-methoxy residue dips more in the binding picket resulted in forming more hydrophobic interactions with lipophilic residues like VAL-89, VAL-523, and LEU-359.

Replacing the 3,4,5-tri-methoxy in A-molecule with –CF3 in J-molecule led to enhancing COX-1 inhibition potency by 1μM and keeping the COX-2 inhibition potency around 0.9 μM. As shown in Figures 3.3-d and 3.4-d, docking studies revealed that the –CF3 group involves more in the COX-1 binding pocket than the tri-methoxy group, so lesser electronic and steric clashes resulted in increasing the potency. The similar interaction pattern of the J-molecule and A-molecule inside the COX-2 binding site is reflected by similar potency.

Figure 3.3

Docking simulation of celecoxib (a), A (b), B (c), and J (d) molecules across the binding location of COX-1 (PDB ID: 3KK6).

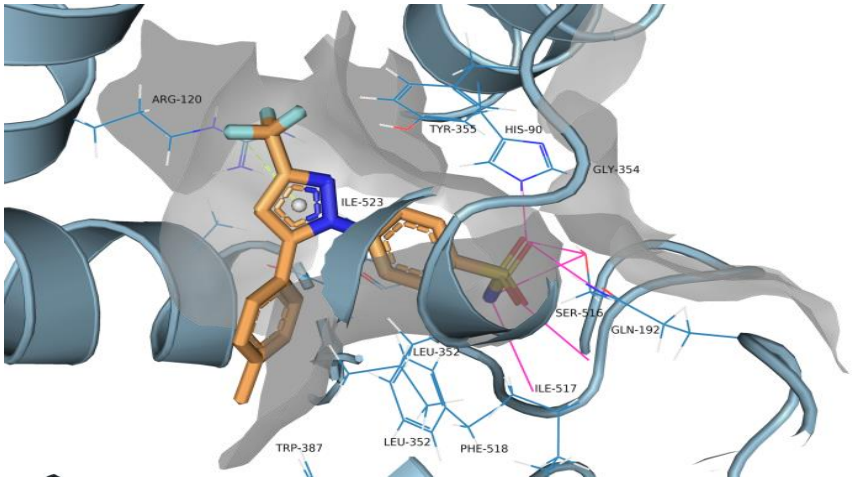

(a) *3D gray surface is used to represent the active site. Ligands are shown as stick structures-orange color. Light-magnet lines represent hydrogen bonds; the light green dashed lines indicate the presence of the Pi-cation bond. The absence of the secondary binding pocket in COX-1 results in rotating the sulfonamide group toward SER-516, Thus the 4-methyl phenyl group generates some steric clashes with the larger amino acid ILE-523 inside COX-1.*

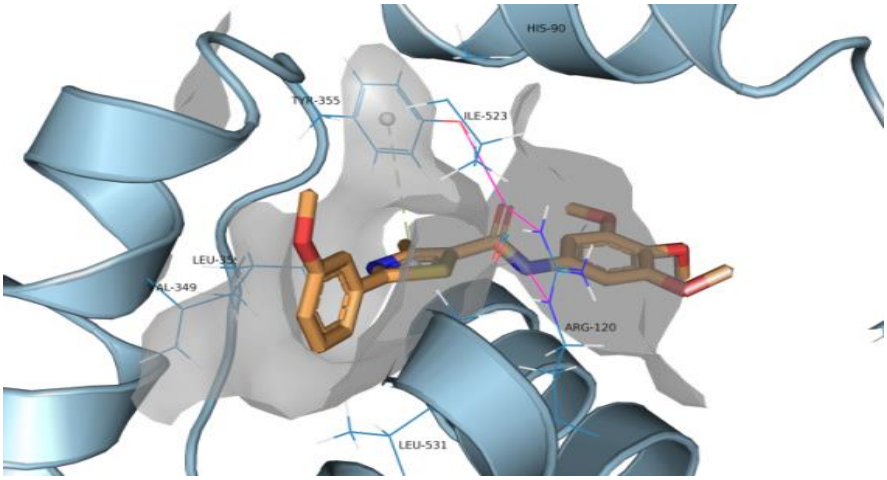

(b) *A-molecule showed a low congruency with the dimensions of the COX-1 binding site, so steric and electronic penalties decrease the COX-1 inhibition potency.*

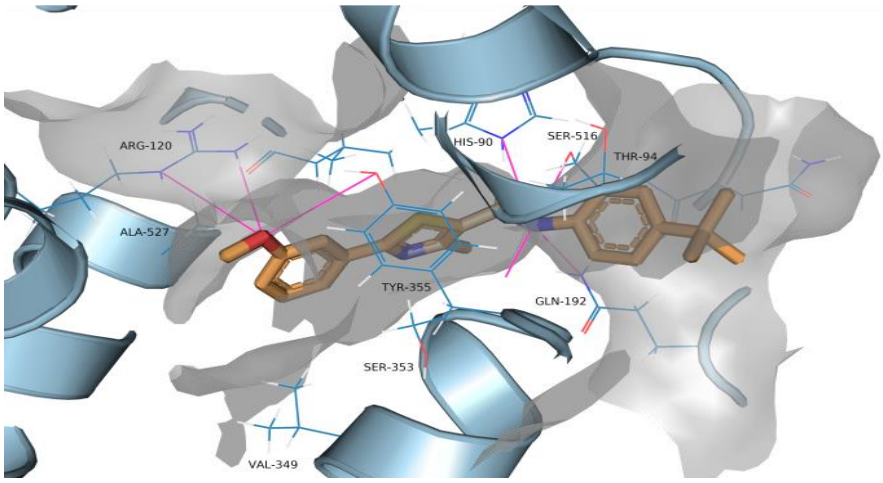

(c) *B-molecule recorded a high inhibition activity against COX-1 by forming 6 favorable hydrogen bonds.*

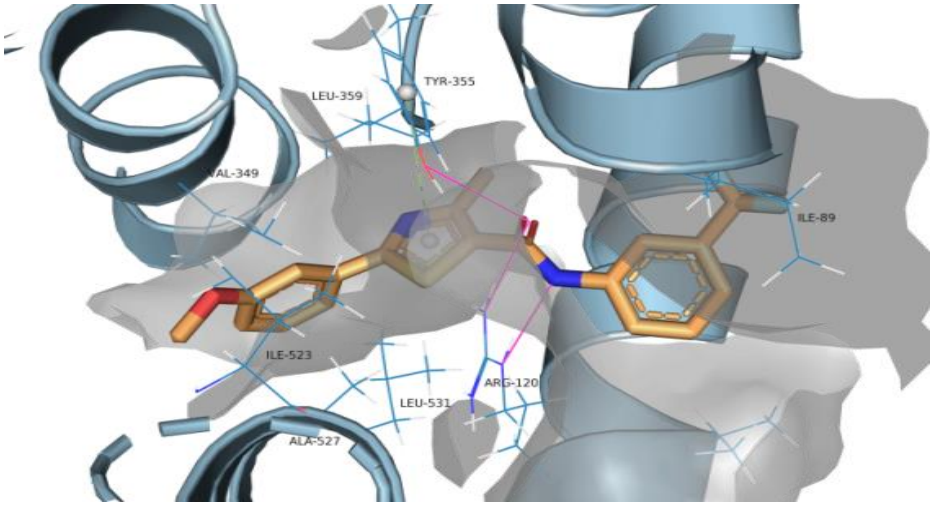

(d) *Replacing the 3,4,5-tri-methoxy in A-molecule with –CF3 in J-molecule led to enhancing COX-1 inhibition potency by 1μM.*

Figure 3.4

Docking simulation of A, B, and J molecules Celecoxib (a), A (b), B (c), and J (d) molecules in the COX-2 (PDB ID: 5KIR).

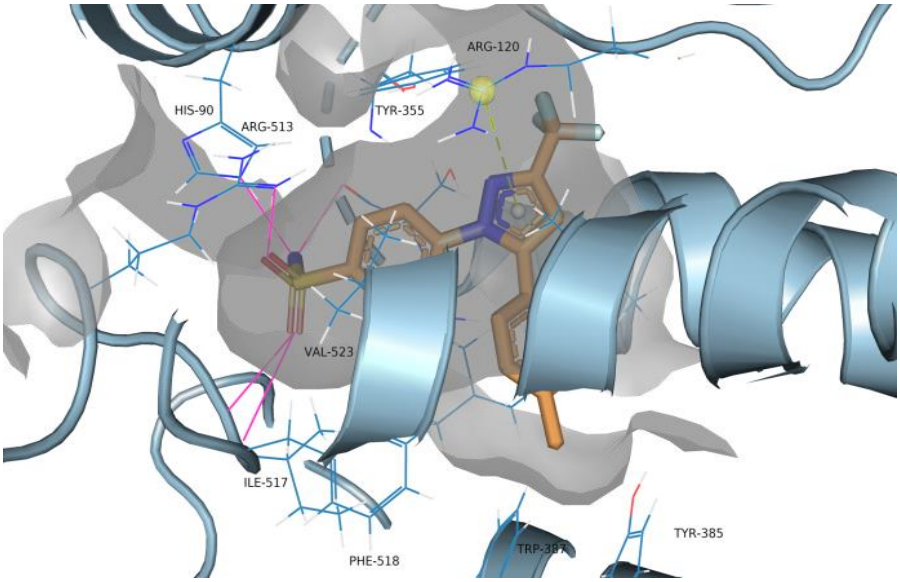

(a) *A 3D gray surface is used to represent the active site (transparency 50%). Ligands are shown as stick structures-orange color. Light-magnet lines represent hydrogen bonds; the light green dashed lines indicate the presence of the Pi-cation bond. Celecoxib showed optimal occupying and interaction pattern within the COX-2 binding site, which involves filling the new generated secondary binding pocking.*

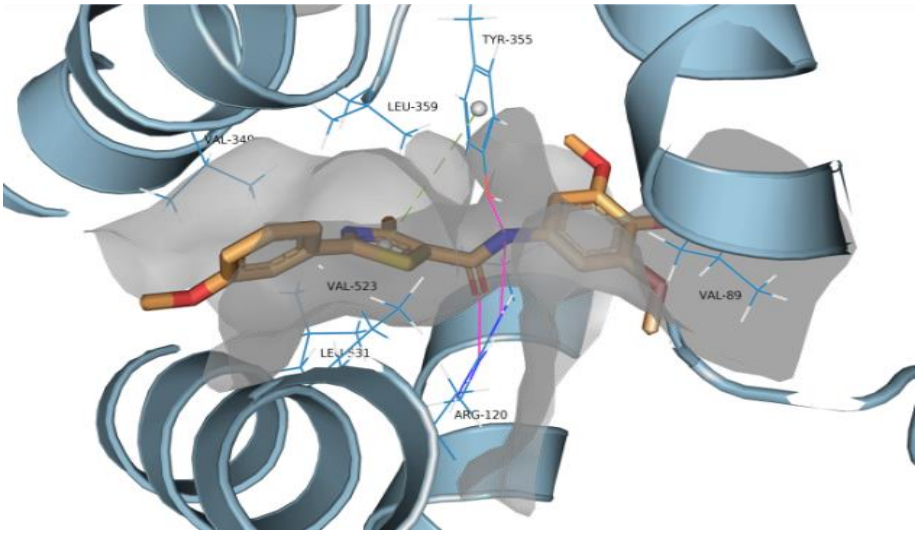

(b) *A-molecule showed similar interaction patterns within the binding site of COX-2,but the 3,4,5 tri-methoxy residue dips more in the binding picket resulted in forming more hydrophobic interactions with lipophilic residues*

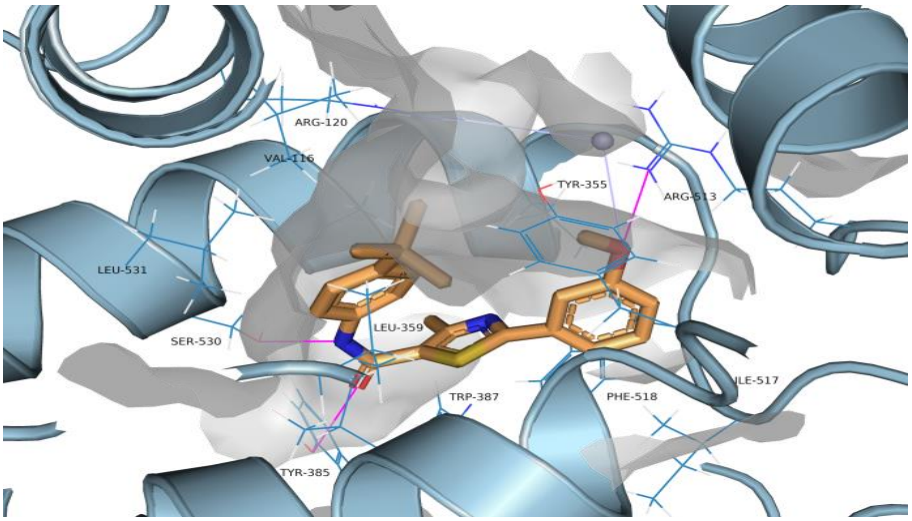

(c) *B-molecule showed its capability to fill the COX-2 binding site optimally, encompassing the available secondary polar binding pocket.*

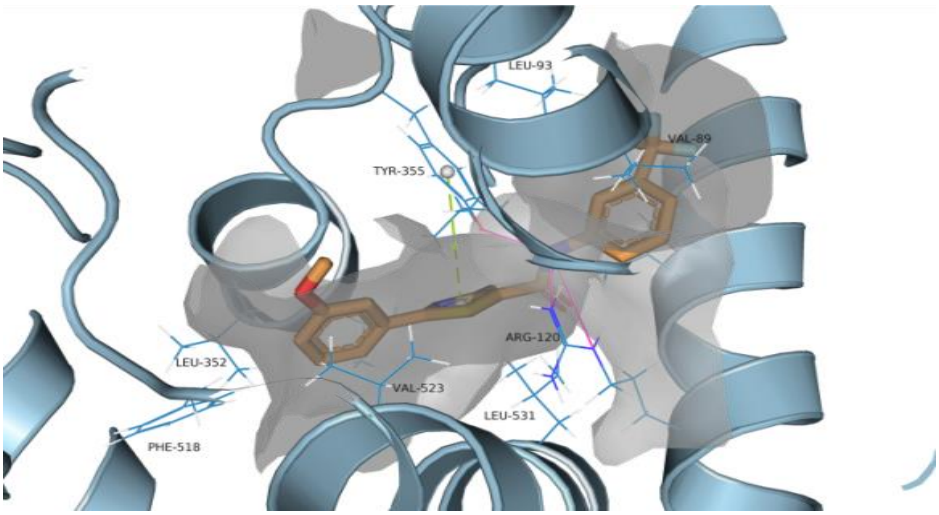

(d) *Replacing the 3,4,5-tri-methoxy in A-molecule with –CF3 in J-molecule led to enhancing keeping the COX-2 inhibition potency around 0.9 μM.*

Table 3

Docking scores of the newly designed ligands within the COX 1 and COX 2 receptors and the free energy calculation (ΔG_{bind}) of ligand-drug complexes using Prime/MM-GBSA

	COX 1		COX 2	
Ligands	docking score	ΔG_{bind}	docking score	ΔG_{bind}
A	-5.59	-50.75	-5.93	-58.07
B	-5.60	-43.39	-8.39	-70.72
J	-6.09	-58.33	-6.93	-62.94
Celecoxib	-10.86	-73.89	-11.28	-80.18

3.3.2 Prime-MM/GBSA Analysis

To investigate the relative binding affinity of the positive control drug (celecoxib) and the three selected ligands (A, B, and J) to COX-1 and COX-2 isozymes, MM/GBSA calculations were performed. Within the binding site of COX-1 isozyme, celecoxib and the three selected molecules showed good binding free energy values (ΔG_{bind}) equaled to -73.89, -50.75, -43.39, and -58.33 Kcal/mol for celecoxib, A, B, and J-molecules, respectively. Making a binding free energy calculation of ligands within the COX-2 binding site resulted in recording ΔG_{bind} values equals to -80.18, -58.07, -70.72, and -62.94 Kcal/mol for celecoxib, A, B, and J, respectively. All the MM-GBSA calculations are summarized in Table 3. As the calculated binding affinity (ΔG_{bind}) of celecoxib is lower than our tested molecules, celecoxib has a stronger affinity to both COX-1 and COX-2 active sites, which is consistence with the recorded XP-Glide docking scores and biological results.

3.3.3 Density Functional Theory Analysis

Frontier orbital theory states that a molecule's stability and reactivity at the receptor binding site (ligand-receptor interactions) or in a chemical reaction could be precisely predicted based on certain features like the symmetries and shapes of HOMO and LUMO orbitals, which are mostly anti-bonding type orbitals [61]. As shown in Figure 3.5, The highest occupied molecular orbital energy (HOMO), and the lowest unoccupied molecular orbital energy (ELUMO), and the HOMO-LUMO energy gap (ΔE) were calculated besides visualizing the HOMO and LUMO maps for the reference drug (celecoxib) and A, B, and J- molecules. Positive lobes are shown by the color red, while the blue color designates negative lobes. These calculated electronic parameters were validated by observing the celecoxib electrostatic potential patterns. and selected

ligands, as shown in Figure 3.6. The HOMO indicates the ability to donate electrons, while LUMO represents the capacity to take electrons. The HOMO-LUMO gap (ΔE) refers to the energy differential between HOMO and LUMO, which determines the optical polarizability, chemical reactivity, kinetic stability, and chemical hardness-softness[62, 63]. Examining the HOMO maps indicates that the electron donor para-methyl diazole ring, 3,4,5-tri-methoxy phenyl, t-butyl phenyl, and 4-methoxy phenyl-thiazole fragments showed the highest electron density.

Hydrophobic interactions are favored for those phenyl rings of the high electron density HOMO fragments. Within the protein binding site, the impact of HOMO energy could be rationalized in terms of many valuable interactions like π---π and π--- σ stacking and charge transfer between aromatic rings of molecules and residues at binding sites. While examining the LUMO profiles indicates that fragments of lower electron density locate over the sulfonamide-phenyl of celecoxib and the thiazole-4-methoxy phenyl fragment of A, B, and J molecules. Suggesting the susceptibility of those parts toward nucleophilic attack.

As summarized in Figure 3.5, calculated HOMO energy values for celecoxib, A, B, and J molecules are -0.240, -0.197, -0.211, and -0.223 eV, respectively. Similarly, the LUMO energy values are -0.059, -0.079, -0.070, and -0.075 eV. The tested ligands' chemical stability and reactivity could be predicted by calculating the HOMO-LUMO gap (ΔE), the calculated ΔE values of celecoxib, A, B, and J molecules equal to 0.181, 0.118, 0.141, and 0.148 eV, respectively. Higher energy gabs indicate higher chemical hardness and lower polarizability (more energy is required for excitement from HOMO to LUMO [64].

As shown in Figure 3.6, the electrostatic potential (ESP) map highlights the regions of negative potential around the oxygen atoms of carbonyl and methoxy groups within A, B, and J molecules and of the sulfone group within celecoxib. Also, the locations with low potential surrounding the nitrogen atoms within the diazole and thiazole rings of celecoxib and our tested ligands were highlighted, respectively. Inspecting the ESP profiles has many beneficial revenues because it influences the interactions between ligands and proteins at an early stage and allows the prediction of the critical sites for optimal binding[65].

Figure 3.5

The celecoxib (a), A (b), B (c), and J (d) molecules' 3D highest occupied molecular orbital (HOMO), lowest unoccupied molecular orbital (LUMO), orbital energy values, and HOMO-LUMO energy gaps (E).

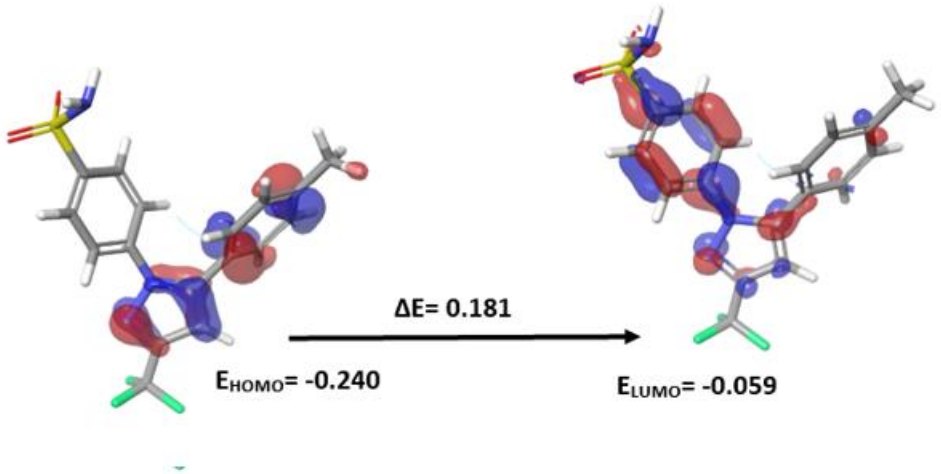

(a) *Positive lobes are shown by the color red, the blue color designates negative lobes. The calculated HOMO energy value for celecoxib was -0.240, the LUMO energy value was -0.059, and the calculated ΔE value was 0.181.*

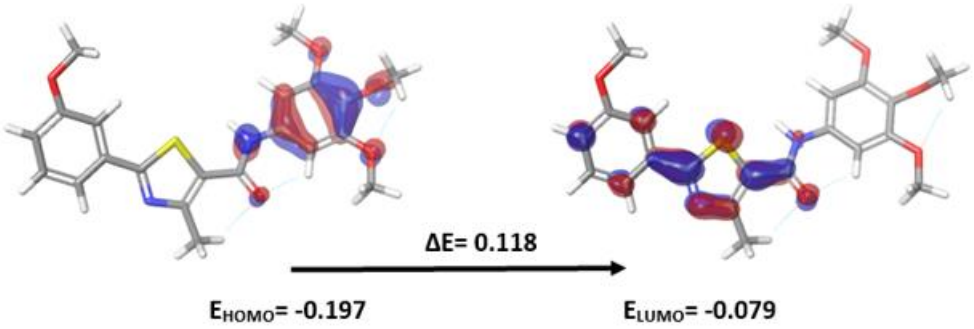

(b) *The calculated HOMO energy value for A-molecule was -0.197, the LUMO energy value was -0.079, and the calculated ΔE value was 0.118.*

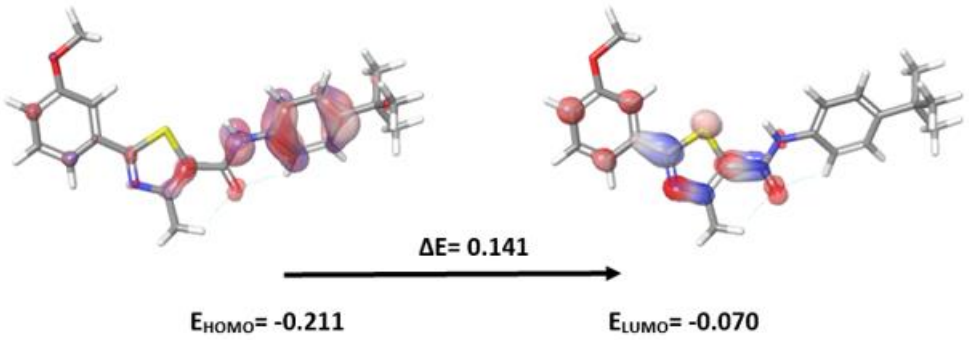

(c) *The calculated HOMO energy value for B-molecule was -0.211, the LUMO energy value was -0.070, and the calculated ΔE value was 0.141.*

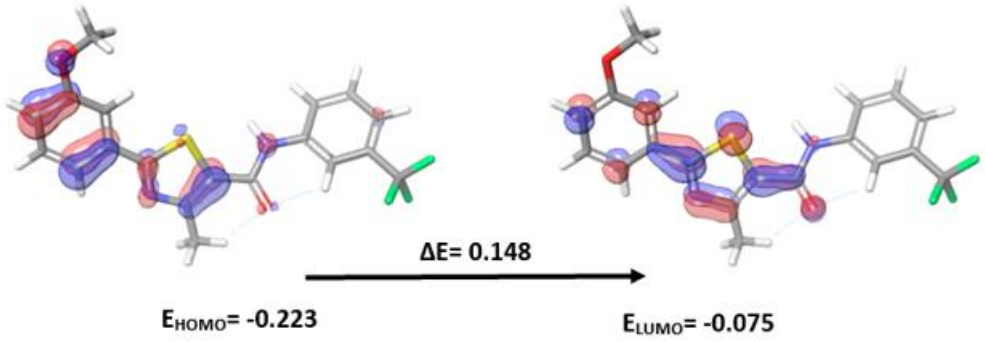

(d) *The calculated HOMO energy value for J-molecule was -0.223, the LUMO energy value was -0.075, and the calculated ΔE value was 0.148.*

Figure 3.6

Electrostatic potential profiles of celecoxib (a), A (b), B (c), and J (d) molecules.

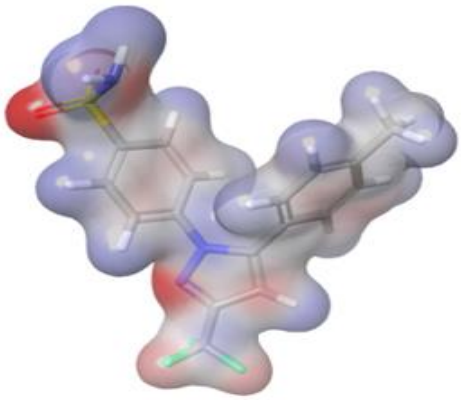

(a) *The electrostatic potential (ESP) map highlights the regions of the sulfone group within celecoxib and the locations with low potential surrounding the nitrogen atoms within the diazole and thiazole rings of celecoxib were highlighted.*

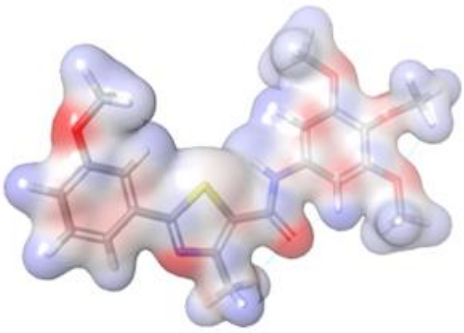

(b) *ESP map highlights the regions of negative potential around the oxygen atoms of carbonyl and methoxy groups within A-molecule and the locations with low potential surrounding the nitrogen atoms within the diazole and thiazole rings were also highlighted.*

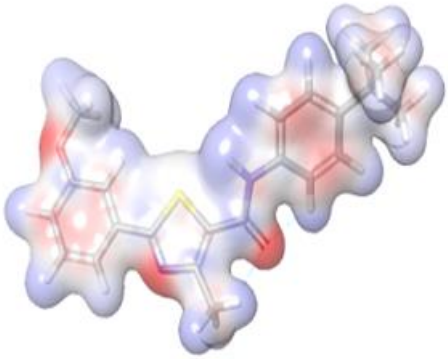

(c) *ESP map highlights the regions of negative potential around the oxygen atoms of carbonyl and methoxy groups within B-molecule and the locations with low potential surrounding the nitrogen atoms within the diazole and thiazole rings were also highlighted.*

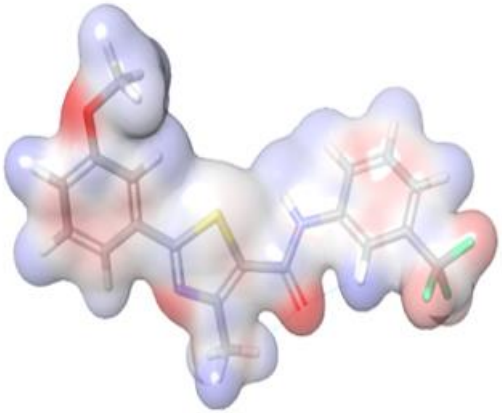

(d) *ESP map highlights the regions of negative potential around the oxygen atoms of carbonyl and methoxy groups within J-molecule and the locations with low potential surrounding the nitrogen atoms within the diazole and thiazole rings were also highlighted.*

3.3.4 ADME-T analysis

Estimating the ADME-T features of the newly developed drugs is a decisive indicator for successful development during the advanced stages of drug processing. Exhibiting unfavorable ADME-T parameters usually is a stumbling block to preceding the drug progression could finally be eliminated. Thus, our newly 10 designed ligands had been subjected to the QikProp module (schrödinger 12.1, LLC, NY), and most incorporated physicochemical and pharmacokinetic parameters (ADME-T calculations) like molecular weight (Mol Mw), accessible surface area for solvents (SASA), polar surface area (PSA), Hydrophilic component of the SASA (FISA), Hydrophobic component of the SASA (FOSA), Total solvent-accessible volume (Volume), π component of the SASA (PISA), Predicted polarizability (QPpolrz), SASA component that is weakly polar (WPSA), predicted human oral absorption, predicted Caco-2 cell permeability (QPPCaco), computed dipole moment (Dipole), number of probable metabolic processes (#metab⁑), octanol/gas partition coefficient (QPlogPoct++), octanol/water partition coefficient (QPlogPo/w), brain/blood partition coefficient (QPlogBB), aqueous solubility (QPlogS), predicted blockage of HERG K+ channels (QPlogHERG), binding to human serum albumin (QPlogKhsa), number of violations of Jorgensen's rule of 3, and number of violations of Lipinski rule of 5 were investigated. All the obtained calculations and the recommended values are listed in Table 4.

Based on ADME-T properties recorded for the tested molecules, all ligands showed optimal pharmacokinetic and physicochemical values within the desirable ranges. However, the predicted aqueous solubility of B, I, and J molecules was slightly lower than the recommended value. As the other investigated parameters are located in the optimal desirable ranges, like the recorded 100% human oral absorption, this minor deviation could be bypassed and compensated. Thus, our newly discovered ligands are suitable for further development as anti-inflammatory drugs based on their observed potential drug-like properties and low toxicity.

Table 4

The ADME-T characteristics of synthetic compounds utilizing the usual mode of the QiKProp module from Schrödinger 12.1, LLC, New York.

		Compounds										Recommended values
		2a	2b	2c	2d	2e	2f	2g	2h	2i	2j	
ADMET parameters	Mol_MW	414.4	380.5	384.4	384.4	370.4	324.3	384.4	384.4	446.5	392.3	130-725
	PSA	76.1	52.7	68.5	69.1	52.7	52.7	68.1	67.9	67.2	52.7	7 – 200
	SASA	726.8	713.3	688.2	686.3	675.9	612.7	690.8	689.6	784.9	664.3	300.0 – 1000.0
	FOSA	440.4	366.4	358.9	357.7	361.8	174.3	356.7	356.9	263.3	175.1	0.0 – 750.0
	FISA	44.8	46.5	44.6	44.8	46.8	46.6	48.3	46.1	45.9	46.6	7.0 – 330.0
	PISA	213.0	271.8	255.9	255.2	297.1	363.4	260.8	261.7	446.1	296.9	0.0 – 450.0
	WPSA	28.5	28.6	28.6	28.4	70.1	28.3	24.9	24.7	29.5	145.6	0.0 – 175.0
	Volume	1280.9	1259.1	1195.4	1195.3	1163.6	1044.3	1204.7	1203.7	1388.3	1142.5	500.0 – 2000.0
	QPpolrz	43.2	44.2	40.9	40.9	40.6	37.1	41.3	41.3	49.8	40.4	13.0 – 70.0
	QPPCaco	3721	3586	3733	3717	3564	3580	3446	3618	3633	3579	<25 poor >500 great
	Percent Human Oral Absorption	100	100	100	100	100	100	100	100	100	100	>80% is high <25% is low
	#metab‡‡	6	3	5	6	3	4	5	6	4	3	1-8
	Dipole	5.66	4.82	5.64	5.61	3.89	4.90	6.87	5.06	7.72	6.58	1.0-12.5
	QPlogPo/w	4.48	5.29	4.25	4.25	4.64	4.05	4.27	4.28	5.78	5.03	-2.0-6.5
	QPlogPoct++	19.38	18.6	18.2	18.2	17.7	16.4	18.6	18.3	21.7	18.2	8.0-35
	QPlogBB	-0.21	-0.10	-0.14	-0.14	-0.01	-0.02	-0.19	-0.16	-0.24	0.24	-3 – 1.2
	QPlogHERG	-6.03	-6.02	-6.12	-6.08	-6.32	-6.30	-6.13	-6.12	-7.43	-6.25	below –5
	QPlogS	-6.03	-6.98	-5.80	-5.77	-6.05	-5.35	-5.83	-5.81	-7.46	-6.77	-6.0-0.5
	QPlogKhsa	0.44	0.93	0.41	0.41	0.57	0.40	0.43	0.43	0.93	0.66	-1.5 – 1.5
	Rule of three	1	1	1	1	1	0	1	1	1	1	<3
	Rule of five	0	1	0	0	0	0	0	0	1	1	<4

Chapter Four

Conclusion

The researcher in this section concludes the results of the thesis. Synthetic chemical 2b was the most effective against the COX-1 enzyme. It also showed potent activity against COX-2 with a selectivity ratio of 1.251. The highest selectivity ratio was (2.766) for the 2a compound against COX-2 with IC_{50} = 0.958 μM regarding celecoxib ratio (23.8) and its IC_{50} against COX-2 =0.002 μM, 2j compound also showed good selectivity towards COX-2 (1.507).

The docking simulation and interaction pattern of the B-molecule displayed the most COX-2 inhibition activity (IC_{50}= 0.19 μM) compared to other newly designed molecules. It showed its ability to optimally fill the COX-2 binding site, including the available secondary polar binding pocket. The high inhibition activity of B-molecule recorded against COX-1 isozyme (IC_{50}=0.239 μM) clarified by forming of 6 favorable hydrogen bonds with TYR-355, HIS-90, ARG-120, GLN-192, SER-353, and SER-516. Also, the *t*-butyl group plays an important role in stabilizing B-Molecule.

Regarding A-molecule molecular docking studies in the binding site of COX-1 and COX-2, the three methoxy substituents do not locate in the binding distances, so pay steric and electronic penalties to result in decreasing the COX-1 inhibition potency, the similar interaction pattern of J-molecule and A-molecule inside the COX-2 binding site is reflected by similar potency.

In the binding site of the COX-1 isozyme, celecoxib and the three selected molecules showed good binding free energy values (ΔG_{bind}). As the calculated binding affinity (ΔG_{bind}) of celecoxib is lower than our tested molecules, celecoxib has a stronger affinity to both COX-1 and COX-2 active sites, which is consistence with the recorded XP-Glide docking scores and biological results. Because the chemical stability and reactivity of the tested ligands could be predicted via calculating the HOMO-LUMO gap (ΔE), the calculated ΔE values of celecoxib, A, B, and J molecules equal to 0.181, 0.118, 0.141, and 0.148 eV, respectively. Higher energy gabs indicate higher chemical hardness and lower polarizability

All ligands showed the optimal pharmacokinetic and physicochemical values within the desirable ranges, and the predicted aqueous solubility of B, A, and J molecules was slightly lower than the recommended value. Because the other inspected parameters are located in the optimal desirable ranges, like the recorded 100% human oral absorption, our newly discovered ligands are suitable for further development as anti-inflammatory drugs based on their observed potential drug-like properties and low toxicity. All newly synthesized compounds did not prove any effects on cancer cells.

List of Abbreviations

Abbreviation	Meaning
#metab‡	Predicted human oral absorption, number of likely metabolic reactions
µl	Microliter
µM	Micro molar
5-FU	5-fluorouracil
ADME-T	Absorption, Distribution, Metabolism, Excretion, and Toxicity
AKI	Acute kidney injury
CC	Cytotoxic Concentration
COX	Cyclooxygenase
DCM	Dichloromethane
DFT	Density-functional theory
DMAP	4-Dimethylaminopyridine
DMEM	Dulbecco's Modified Eagle's Medium
DMSO	Dimethyl sulfoxide
DMSO-d_6	Dimethyl sulfoxide-d_6
DPBS	Dulbecco's phosphate-buffered saline
EC	Electrical conductivity
EDCI	1-Ethyl-3-(3-dimethylaminopropyl) carbodiimide
E_{Homo}	Energy of the Highest Occupied Molecular Orbital
E_{Lumo}	Energy of the Lowest Unoccupied Molecular Orbital
EtOAc	Ethyl acetate
FDA	Food and drug administration
FISA	Hydrophilic component of the SASA
FOSA	Hydrophobic component of the SASA
HCL32%	Hydrochloric acid 32%
HIV	Human immunodeficiency virus
HRMS	High Resolution Mass Spectrometry
hrs	Hour or Hours
HT29	Human colorectal adenocarcinoma cell line with epithelial morphology

IC_{50}	The half maximal Inhibitory concentration
ILE-517	Isoleucine
LEU-531	Leucine
mg	Milligram
MHz	Megahertz
MM-GBSA	Molecular mechanics with generalized Born and surface area solvation
mmole	Millimole
MTS	3-(4,5-dimethylthiazol-2-yl)-5-(3-carboxymethoxyphenyl)-2-(4-sulfophenyl)-2H-tetrazolium
MW	Molecular weight
nM	Nano molar
NMR	Nuclear Magnetic Resonance
NSAIDS	Non steroid anti-inflammatory drugs
^{o}C	Celsius Degree
OPLS	Optimized Potentials for Liquid Simulations
PDB	Protein Data Bank
PG	Prostaglandin
PGC-1 alpha	Peroxisome proliferator-activated receptor-gamma coactivator 1 alpha
PGG2	Prostaglandin G2
PGH2	Prostaglandin H2
PGI2	Prostacyclin
pH	Potential of hydrogen
PHE-518	Phenylalanine
PISA	π component of the SASA
PLID	Protein-ligand interaction profiler
QPlogBB	Brain/blood partition coefficient
QPlogHERG	Predicted blockage of HERG K+ channels
QPlogKhsa	Binding to human serum albumin
QPlogPo/w	Octanol/water partition coefficient
QPlogPoct++	Octanol/gas partition coefficient
QPlogS	Aqueous solubility

QPPCaco	Predicted Caco-2 cell permeability
QPpolrz	Predicted polarizability
R_f	Retention factor
RMSD	Root mean square deviation
ROS	Reactive oxygen species
Rpm	Round per minute
RPMI-1640	Roswell Park Memorial Institute Medium
SASA	Solvent accessible surface area
SER-530	Serine residue in the cyclooxygenase (COX) active site
SI	Selectivity index
SIRT1	Sirtuin
TLC	Thin layer chromatography
TXA2	Thromboxane A2
TYR-385	Tyrosine-385
UV-Vis	Ultraviolet-Visible
VAL-116	Valine
WPSA	Weakly polar component of the SASA

References

[1] T Chhabria, M., et al., *Thiazole: A review on chemistry, synthesis and therapeutic importance of its derivatives.* Current topics in medicinal chemistry, 2016. 16(26): p. 2841-2862.

[2] Paudel, A., et al., *A novel spiro-heterocyclic compound identified by the silkworm infection model inhibits transcription in Staphylococcus aureus.* Frontiers in microbiology, 2017. 8: p. 712.

[3] Al-Mulla, A., *A review: biological importance of heterocyclic compounds.* Der Pharma Chemica, 2017. 9(13): p. 141-147.

[4] Ejaz, P., K. Bhojani, and V. Joshi, *NSAIDs and kidney.* Japi, 2004. 52(632-640): p. 371.

[5] Ghlichloo, I. and V. Gerriets, *Nonsteroidal anti-inflammatory drugs (NSAIDs).* 2019.

[6] Day, R.O. and G.G. Graham, *Non-steroidal anti-inflammatory drugs (NSAIDs).* Bmj, 2013. 346.

[7] Todd, P.A. and S.P. Clissold, *Naproxen.* Drugs, 1990. 40(1): p. 91-137.

[8] Todd, P.A. and E.M. Sorkin, *Diclofenac sodium.* Drugs, 1988. 35(3): p. 244-285.

[9] Clemett, D. and K.L. Goa, *Celecoxib.* Drugs, 2000. 59(4): p. 957-980.

[10] Petrou, A., M. Fesatidou, and A. Geronikaki, *Thiazole ring—A biologically active scaffold.* Molecules, 2021. 26(11): p. 3166.

[11] Kashyap, S.J., et al., *Thiazoles: having diverse biological activities.* Medicinal Chemistry Research, 2012. 21(8): p. 2123-2132.

[12] Borcea, A.-M., et al., *An overview of the synthesis and antimicrobial, antiprotozoal, and antitumor activity of thiazole and bisthiazole derivatives.* Molecules, 2021. 26(3): p. 624.

[13] Leoni, A., et al., *Imidazo [2, 1-b] Thiazole: Introduction, Current and Perspective.* Bioenergetics, 2017. 6(151): p. 2.

[14] Li, X., *SIRT1 and energy metabolism.* Acta Biochim Biophys Sin, 2013. 45(1): p. 51-60.

[15] Vu, C.B., et al., *Discovery of imidazo [1, 2-b] thiazole derivatives as novel SIRT1 activators.* Journal of medicinal chemistry, 2009. 52(5): p. 1275-1283.

[16] Lee, M.-S., et al., *Ginsenoside Rc, an active component of Panax ginseng, stimulates glucose uptake in C2C12 myotubes through an AMPK-dependent mechanism.* Journal of ethnopharmacology, 2010. 127(3): p. 771-776.

[17] Huang, Q., et al., *A SIRT1 activator, ginsenoside Rc, promotes energy metabolism in cardiomyocytes and neurons.* Journal of the American Chemical Society, 2021. 143(3): p. 1416-1427.

[18] Kumar, K.A. and P. Jayaroopa, *Pyrazoles: synthetic strategies and their pharmaceutical applications-an overview.* International Journal of PharmTech Research, 2013. 5(4): p. 1473-1486.

[19] Ebenezer, O., M. Shapi, and J.A. Tuszynski, *A Review of the Recent Development in the Synthesis and Biological Evaluations of Pyrazole Derivatives.* Biomedicines, 2022. 10(5): p. 1124.

[20] Liu, J.-J., et al., *Pyrazole derivatives as antitumor, anti-inflammatory and antibacterial agents.* Mini reviews in medicinal chemistry, 2013. 13(13): p. 1957-1966.

[21] Abdellatif, K.R., et al., *Non-acidic 1, 3, 4-trisubstituted-pyrazole derivatives as lonazolac analogs with promising COX-2 selectivity, anti-inflammatory activity and gastric safety profile.* Bioorganic Chemistry, 2018. 77: p. 568-578.

[22] Onoa, G., et al., *Structural and cytotoxic study of new Pt (II) and Pd (II) complexes with the bi-heterocyclic ligand mepirizole.* Journal of inorganic biochemistry, 1999. 75(3): p. 205-212.

[23] Abrigach, F. and R. Touzani, *Pyrazole derivatives with NCN junction and their biological activity: A review.* Med. chem, 2016. 6: p. 292-298.

[24] Karrouchi, K., et al., *Synthesis and pharmacological activities of pyrazole derivatives: A review.* Molecules, 2018. 23(1): p. 134.

[25] Yerragunta, V., et al., *Pyrazole and its biological activity.* PharmaTutor, 2014. 2(1): p. 40-48.

[26] Zarghi, A. and S. Arfaei, *Selective COX-2 inhibitors: a review of their structure-activity relationships.* Iranian journal of pharmaceutical research: IJPR, 2011. 10(4): p. 655.

[27] Assali, M., et al., *Synthesis, biological activity, and molecular modeling studies of pyrazole and triazole derivatives as selective COX-2 inhibitors.* Journal of Chemistry, 2020. 2020.

[28] Altaf, A.A., et al., *A review on the medicinal importance of pyridine derivatives.* J. Drug Des. Med. Chem, 2015. 1(1): p. 1-11.

[29] Scriven, E.F. and R. Murugan, *Pyridine and pyridine derivatives.* Kirk-Othmer Encyclopedia of Chemical Technology, 2000.

[30] Mohammad Abu-Taweel, G., et al., *Medicinal Importance and Chemosensing Applications of Pyridine Derivatives: A Review.* Critical Reviews in Analytical Chemistry, 2022: p. 1-18.

[31] Vessally, E., et al., *New page to access pyridine derivatives: synthesis from N-propargylamines.* RSC advances, 2016. 6(75): p. 71662-71675.

[32] Ahmadi, M., et al., *Non-steroidal anti-inflammatory drugs: recent advances in the use of synthetic COX-2 inhibitors.* RSC Medicinal Chemistry, 2022.

[33] Hawkey, C., *COX-1 and COX-2 inhibitors.* Best Practice & Research Clinical Gastroenterology, 2001. 15(5): p. 801-820.

[34] Knights, K.M., A.A. Mangoni, and J.O. Miners, *Defining the COX inhibitor selectivity of NSAIDs: implications for understanding toxicity.* Expert review of clinical pharmacology, 2010. 3(6): p. 769-776.

[35] Munn, L.L., *Cancer and inflammation.* Wiley Interdisciplinary Reviews: Systems Biology and Medicine, 2017. 9(2): p. e1370.

[36] Yu, T., X. Lao, and H. Zheng, *Influencing COX-2 activity by COX related pathways in inflammation and cancer.* Mini reviews in medicinal chemistry, 2016. 16(15): p. 1230-1243.

[37] Gerstenfeld, L.C. and T.A. Einhorn, *COX inhibitors and their effects on bone healing.* Expert opinion on drug safety, 2004. 3(2): p. 131-136.

[38] Klomjit, N. and P. Ungprasert, *Acute kidney injury associated with non-steroidal anti-inflammatory drugs.* European Journal of Internal Medicine, 2022.

[39] Drazen, J.M., *COX-2 inhibitors--a lesson in unexpected problems.* New England Journal of Medicine, 2005. 352(11): p. 1131-1132.

[40] Berman, H.M., et al., *The protein data bank.* Nucleic acids research, 2000. 28(1): p. 235-242.

[41] Impact, S., *LLC, New York, NY; Prime, Schrödinger, LLC, New York, NY (2021).* Google Scholar There is no corresponding record for this reference.

[42] Friesner, R.A., et al., *Glide: a new approach for rapid, accurate docking and scoring. 1. Method and assessment of docking accuracy.* Journal of medicinal chemistry, 2004. 47(7): p. 1739-1749.

[43] Halgren, T.A., et al., *Glide: a new approach for rapid, accurate docking and scoring. 2. Enrichment factors in database screening.* Journal of medicinal chemistry, 2004. 47(7): p. 1750-1759.

[44] Adasme, M.F., et al., *PLIP 2021: expanding the scope of the protein–ligand interaction profiler to DNA and RNA.* Nucleic acids research, 2021. 49(W1): p. W530-W534.

[45] Schrödinger, L., *The PyMOL molecular graphics system, version 1.3 r1*. 2010, August.

[46] Li, J., et al., *The VSGB 2.0 model: a next generation energy model for high resolution protein structure modeling.* Proteins: Structure, Function, and Bioinformatics, 2011. 79(10): p. 2794-2812.

[47] Jaguar, V., *9.1 Schrödinger Suite Release 2016-1*. Schrödinger, LLC: New York, NY, USA, 2016.

[48] Bochevarov, A.D., et al., *Jaguar: A high-performance quantum chemistry software program with strengths in life and materials sciences.* International Journal of Quantum Chemistry, 2013. 113(18): p. 2110-2142.

[49] Gill, P.M., et al., *The performance of the Becke—Lee—Yang—Parr (B—LYP) density functional theory with various basis sets.* Chemical Physics Letters, 1992. 197(4-5): p. 499-505.

[50] Lee, C., W. Yang, and R.G. Parr, *Development of the Colle-Salvetti correlation-energy formula into a functional of the electron density.* Physical review B, 1988. 37(2): p. 785.

[51] Stephens, P.J., et al., *Ab initio calculation of vibrational absorption and circular dichroism spectra using density functional force fields.* The Journal of physical chemistry, 1994. 98(45): p. 11623-11627.

[52] Nassabeh, N., M. Tran, and P.E. Fleming, *Dissociation of the ethyl radical: an exercise in computational chemistry.* Journal of Chemical Education, 2014. 91(8): p. 1248-1253.

[53] Clare, B.W., *Charge transfer complexes and frontier orbital energies in QSAR: a congeneric series of electron acceptors.* Journal of Molecular Structure: Theochem, 1995. 337(2): p. 139-150.

[54] Zhan, C.-G., J.A. Nichols, and D.A. Dixon, *Ionization potential, electron affinity, electronegativity, hardness, and electron excitation energy: molecular properties from density functional theory orbital energies.* The Journal of Physical Chemistry A, 2003. 107(20): p. 4184-4195.

[55] Zheng, Y., et al., *Design, synthesis, quantum chemical studies and biological activity evaluation of pyrazole–benzimidazole derivatives as potent Aurora A/B kinase inhibitors.* Bioorganic & Medicinal Chemistry Letters, 2013. 23(12): p. 3523-3530.

[56] Zhou, Z. and R.G. Parr, *Activation hardness: new index for describing the orientation of electrophilic aromatic substitution.* Journal of the American Chemical Society, 1990. 112(15): p. 5720-5724.

[57] Elekofehinti, O.O., et al., *Identification of main protease of coronavirus SARS-CoV-2 (Mpro) Inhibitors from Melissa officinalis.* Current Drug Discovery Technologies, 2021. 18(5): p. 38-52.

[58] Bergin, E., *Substituting methoxy groups.* Nature Chemistry, 2014. 6(11): p. 947-947.

[59] Sommer, L.H. and L.J. Tyler, *Steric Effects of the t-Butyl Group in Organosilicon Compounds1*. Journal of the American Chemical Society, 1954. 76(4): p. 1030-1033.

[60] O'Connor, M.J., et al., *Superelectrophiles and the effects of trifluoromethyl substituents.* Journal of the American Chemical Society, 2010. 132(10): p. 3266-3267.

[61] Crisan, L., et al., *Diarylthiazole and diarylimidazole selective COX-1 inhibitor analysis through pharmacophore modeling, virtual screening, and DFT-based approaches.* Structural Chemistry, 2019. 30(6): p. 2311-2326.

[62] Asiri, A.M., et al., *Synthesis, molecular conformation, vibrational and electronic transition, isometric chemical shift, polarizability and hyperpolarizability analysis of 3-(4-Methoxy-phenyl)-2-(4-nitro-phenyl)-acrylonitrile: a combined experimental and theoretical analysis.* Spectrochimica Acta Part A: Molecular and Biomolecular Spectroscopy, 2011. 82(1): p. 444-455.

[63] Kosar, B. and C. Albayrak, *Spectroscopic investigations and quantum chemical computational study of (E)-4-methoxy-2-[(p-tolylimino) methyl] phenol.* Spectrochimica Acta Part A: Molecular and Biomolecular Spectroscopy, 2011. 78(1): p. 160-167.

[64] Parr, R.G. and P.K. Chattaraj, *Principle of maximum hardness.* Journal of the American Chemical Society, 1991. 113(5): p. 1854-1855.

[65] Kenny, P.W., *Hydrogen bonding, electrostatic potential, and molecular design.* Journal of chemical information and modeling, 2009. 49(5): p. 1234-1244.

Appendices

Appendix A

NMR spectrums (^{1}H-NMR and ^{13}C-NMR) for thiazole-carboxamide derivatives compounds

2a

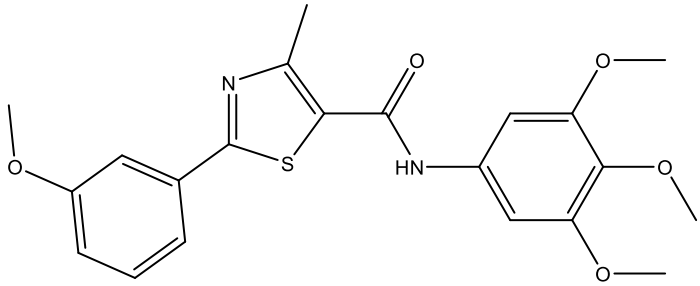

^{1}H-NMR

RS-1

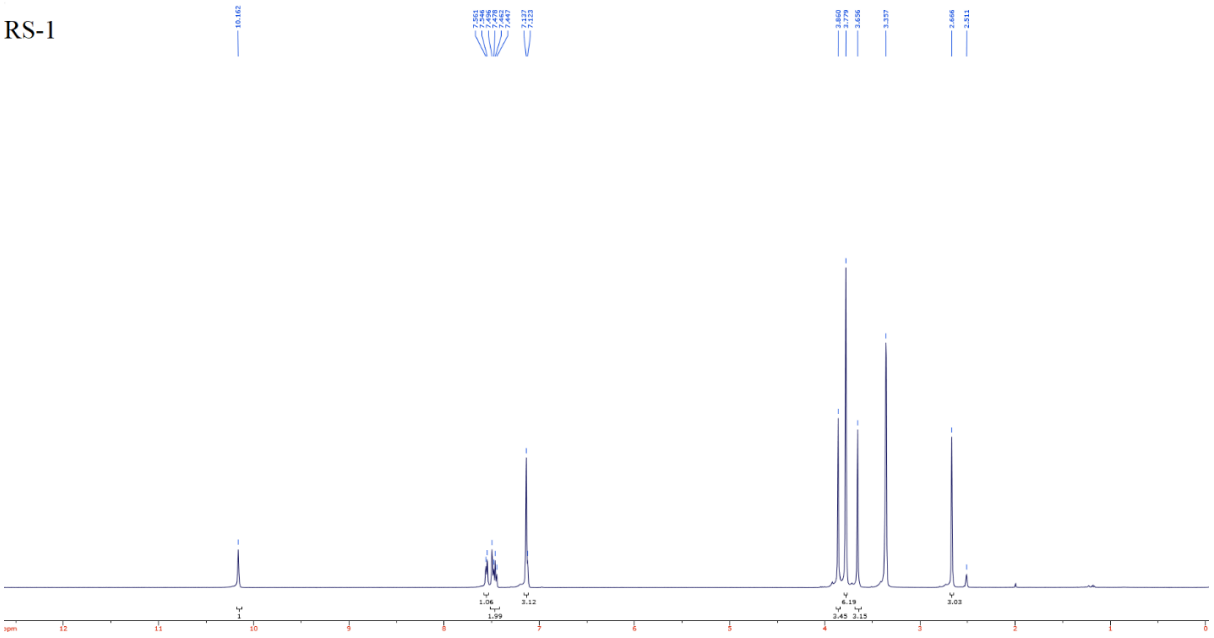

^{13}C-NMR

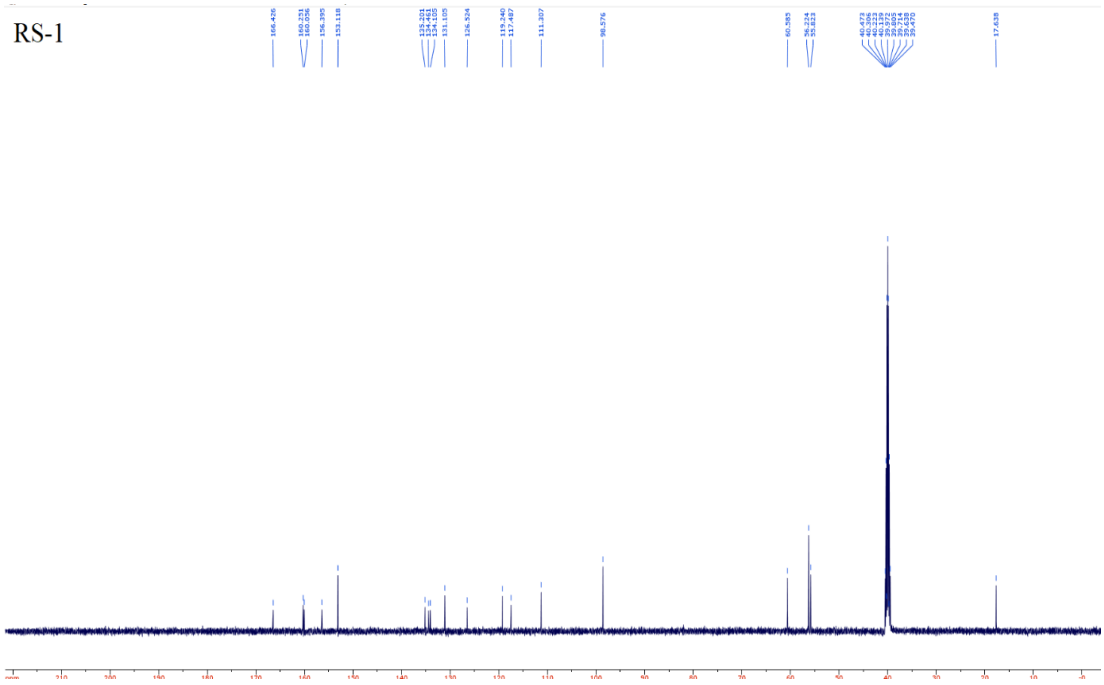

2b

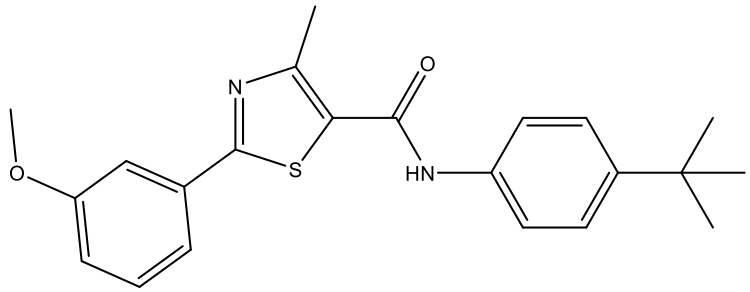

^{1}H-NMR

RS-2

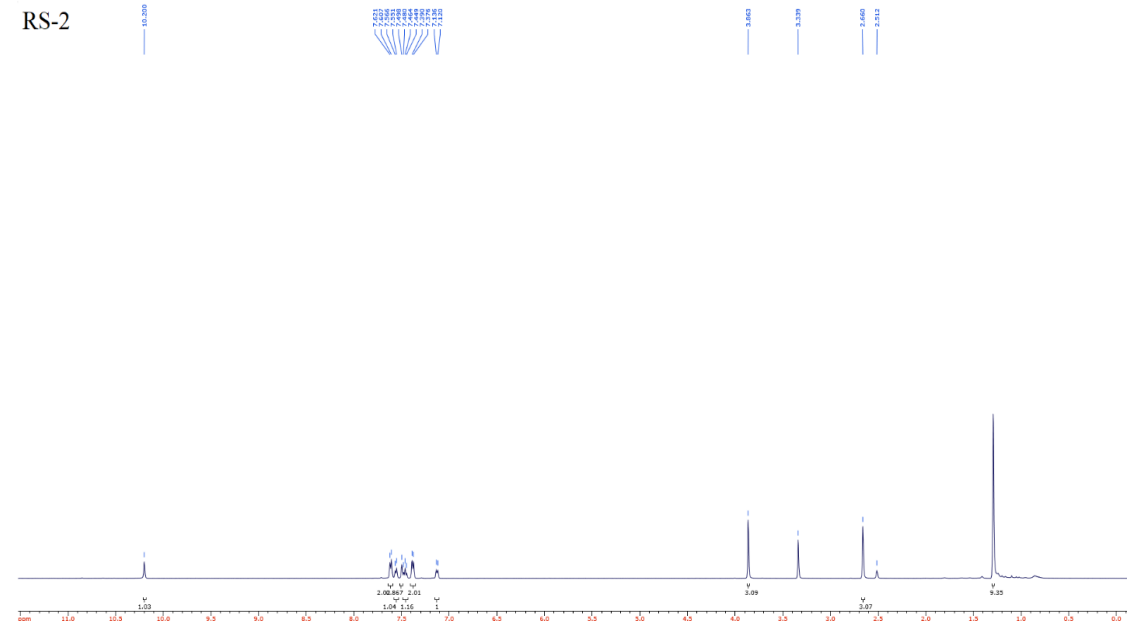

RS-2

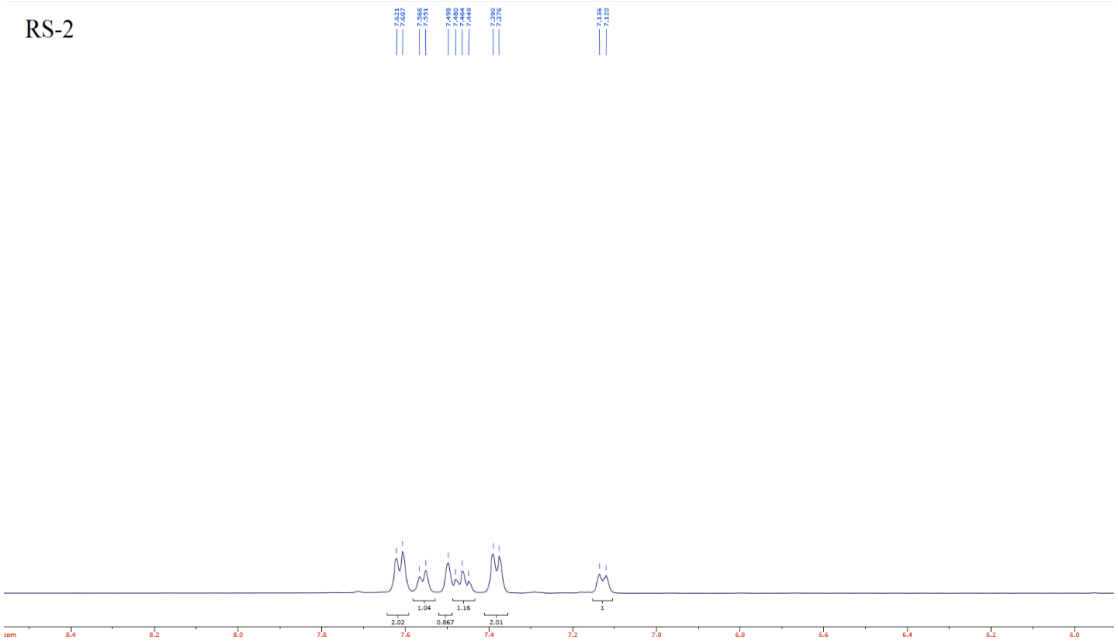

^{13}C-NMR

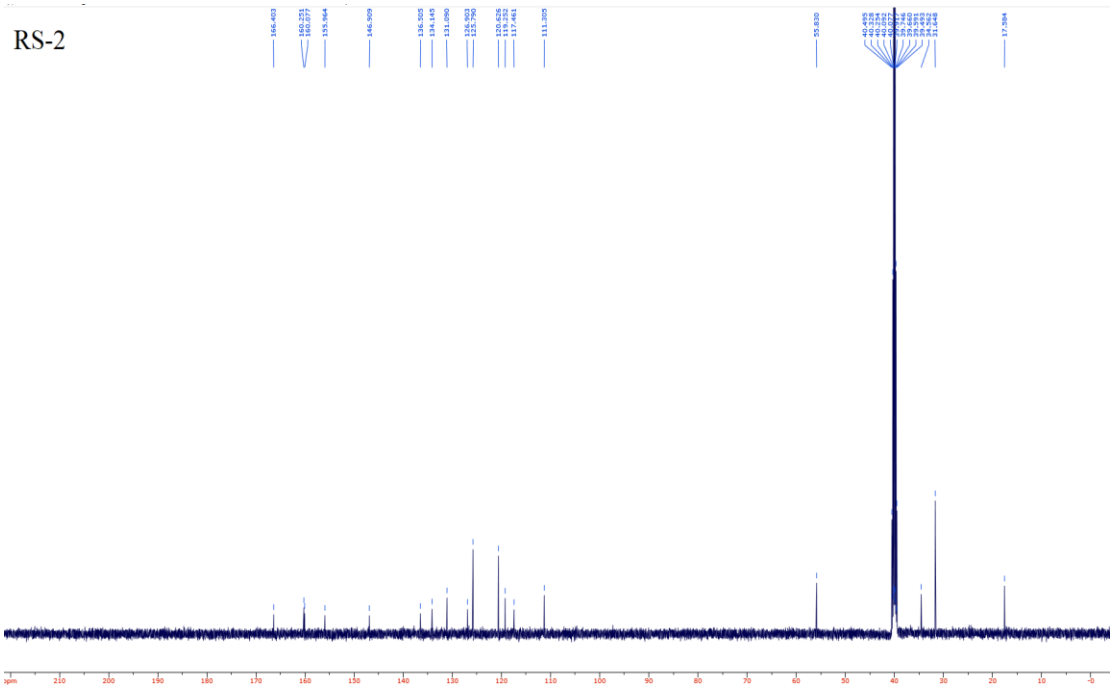

2c

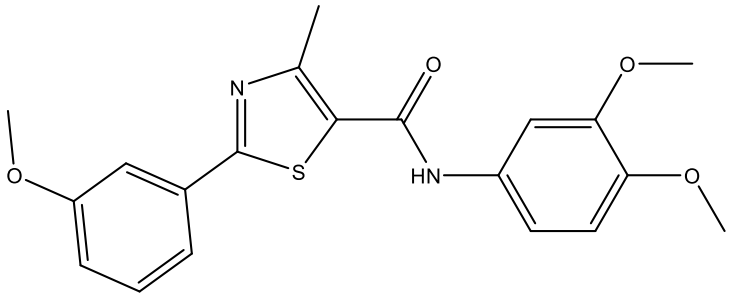

^{1}H-NMR

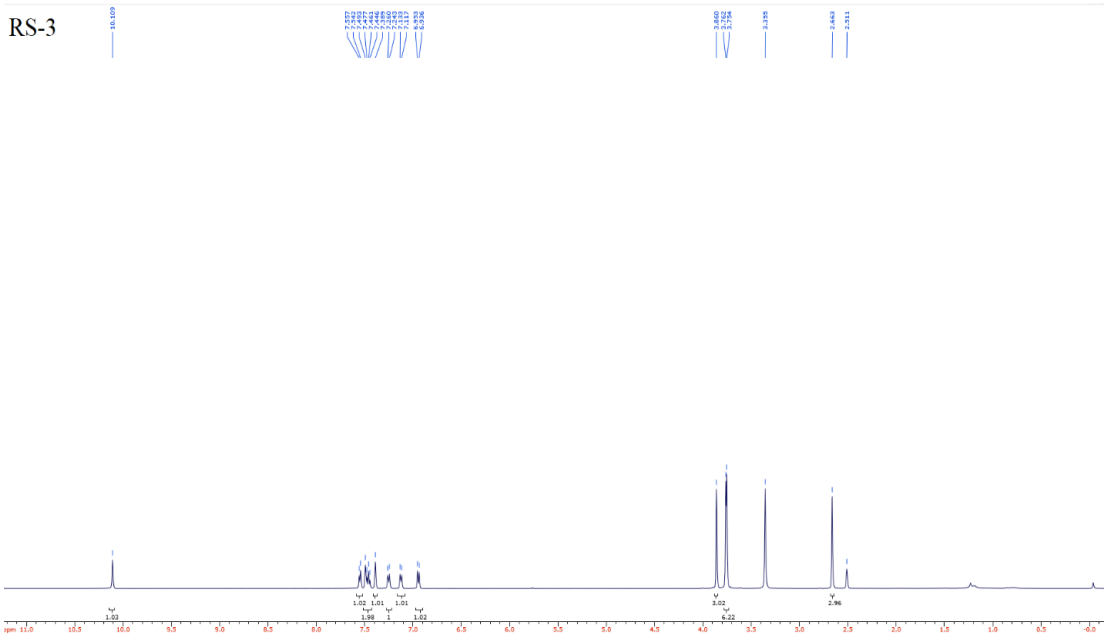

^{13}C-NMR

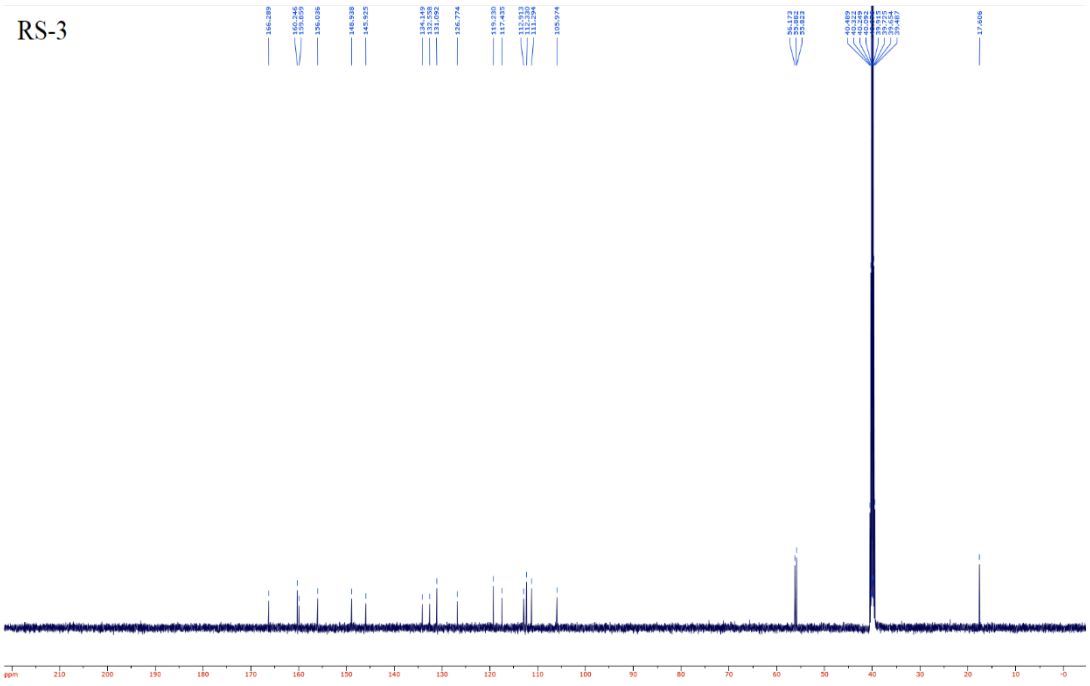

2d

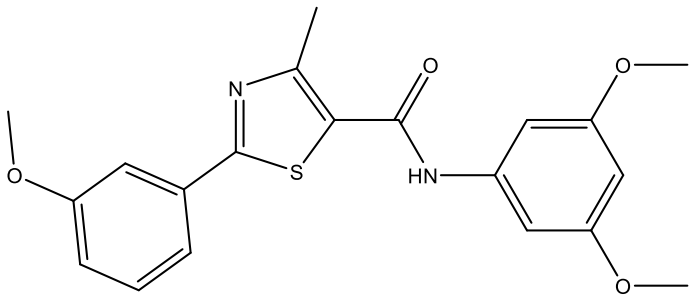

^{1}H-NMR

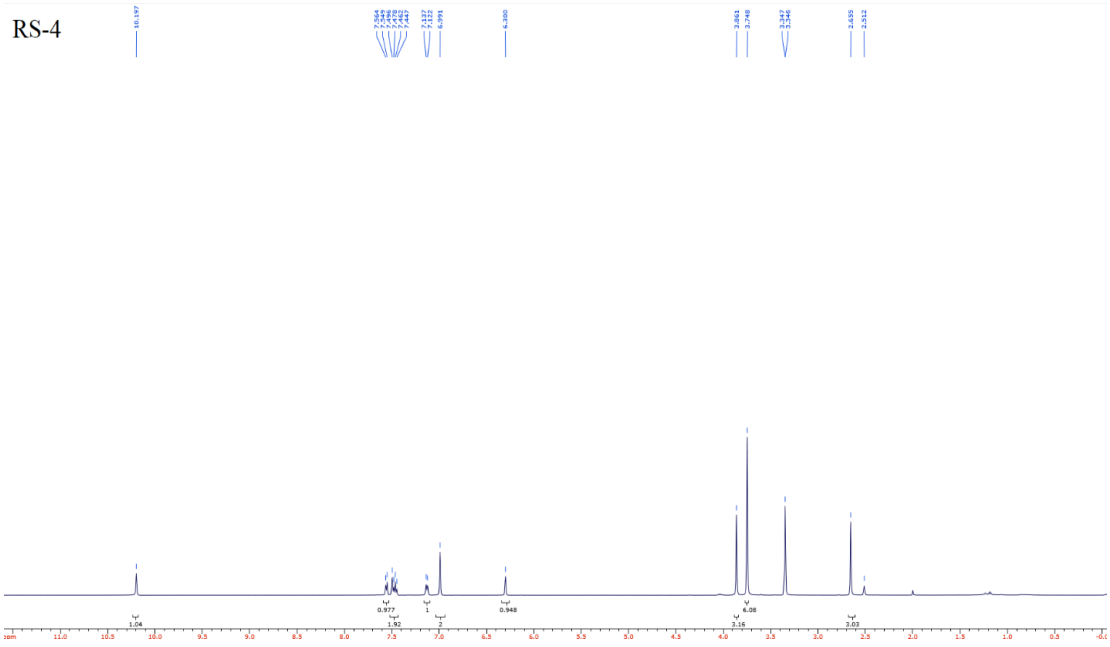

^{13}C-NMR

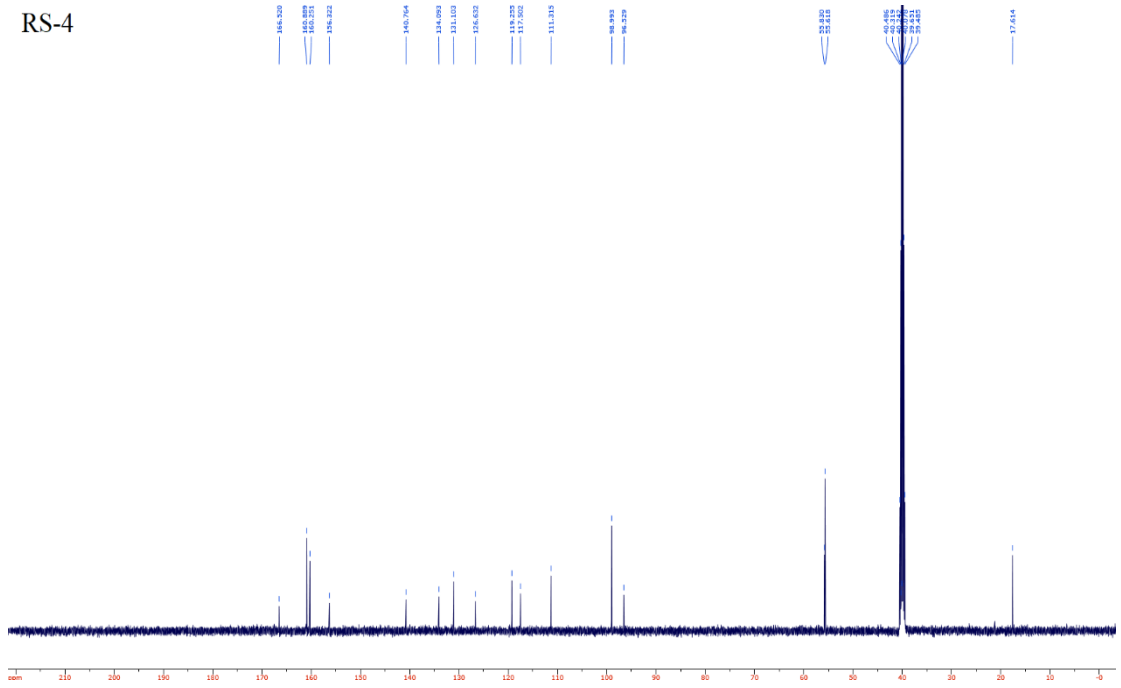

2e

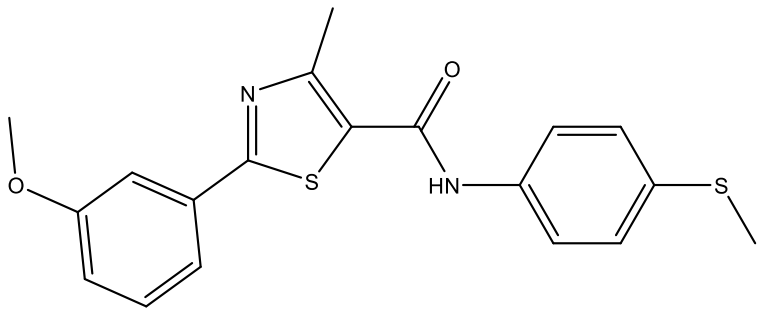

^{1}H-NMR

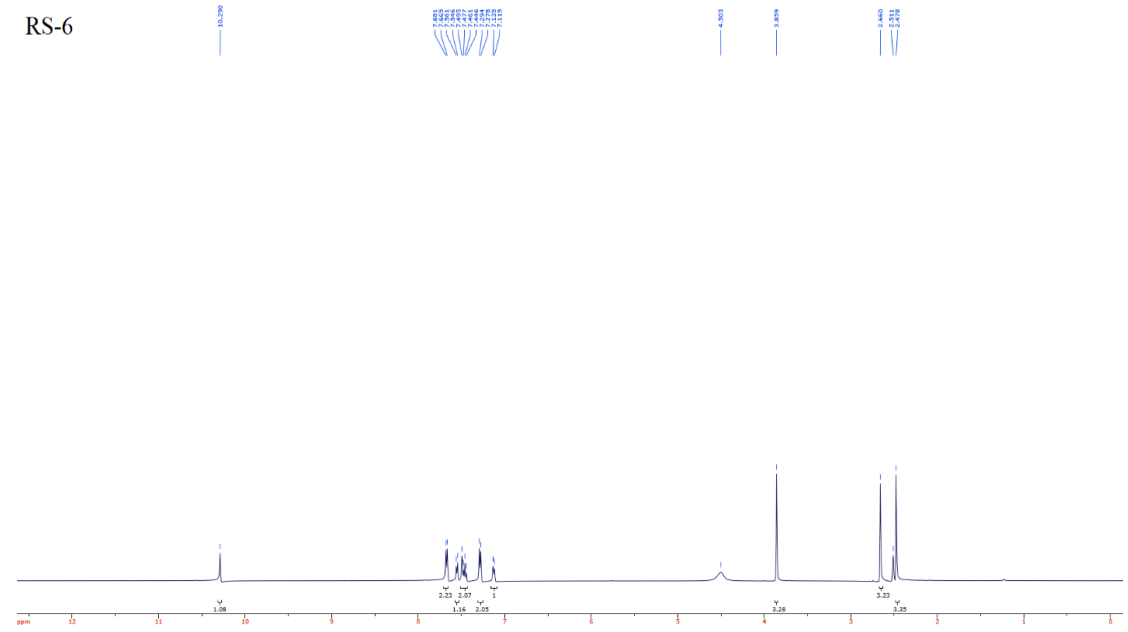

^{13}C-NMR

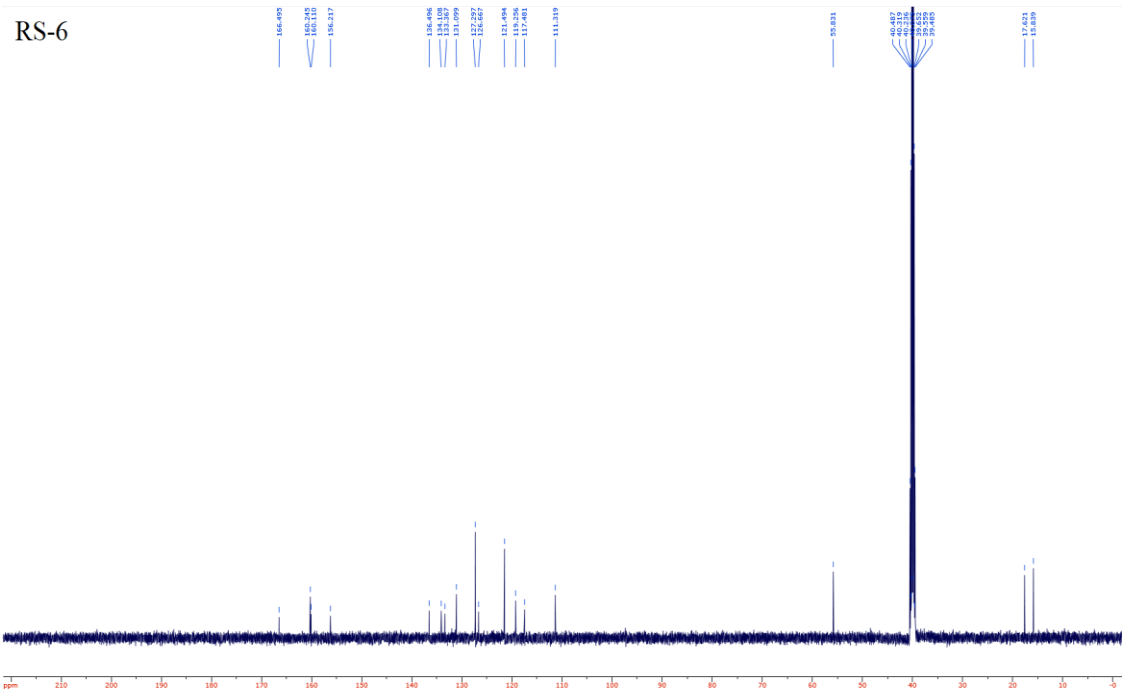

2f

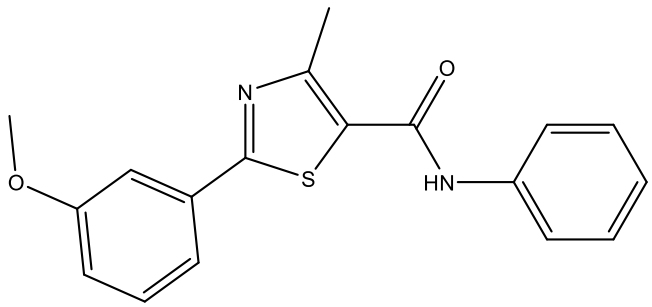

^{1}H-NMR

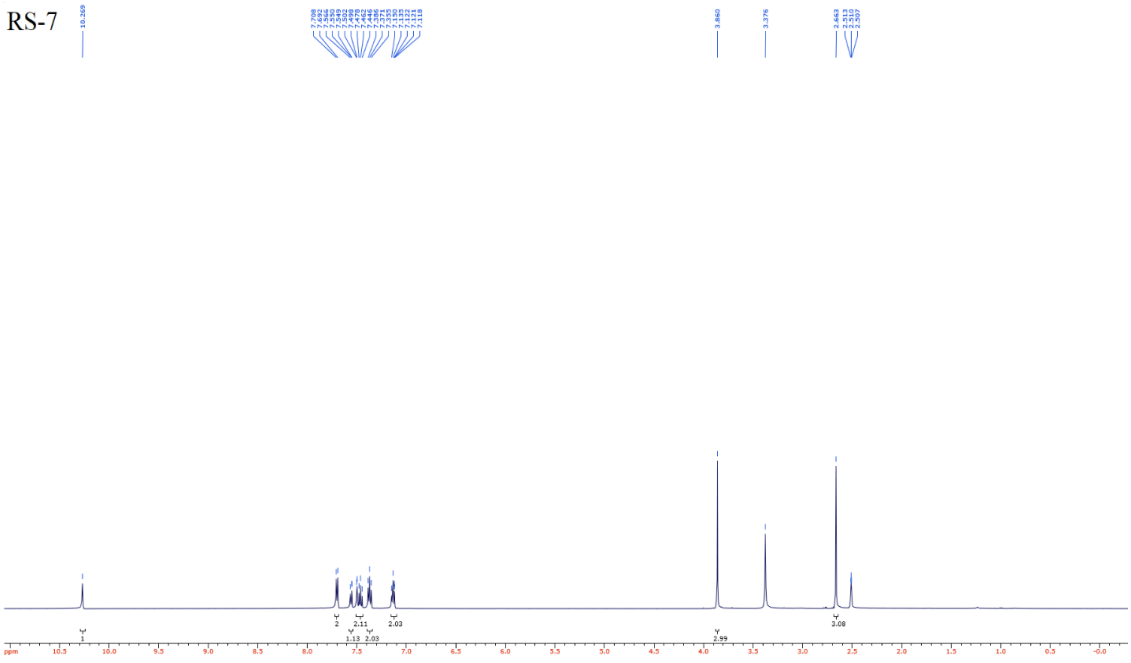

^{13}C-NMR

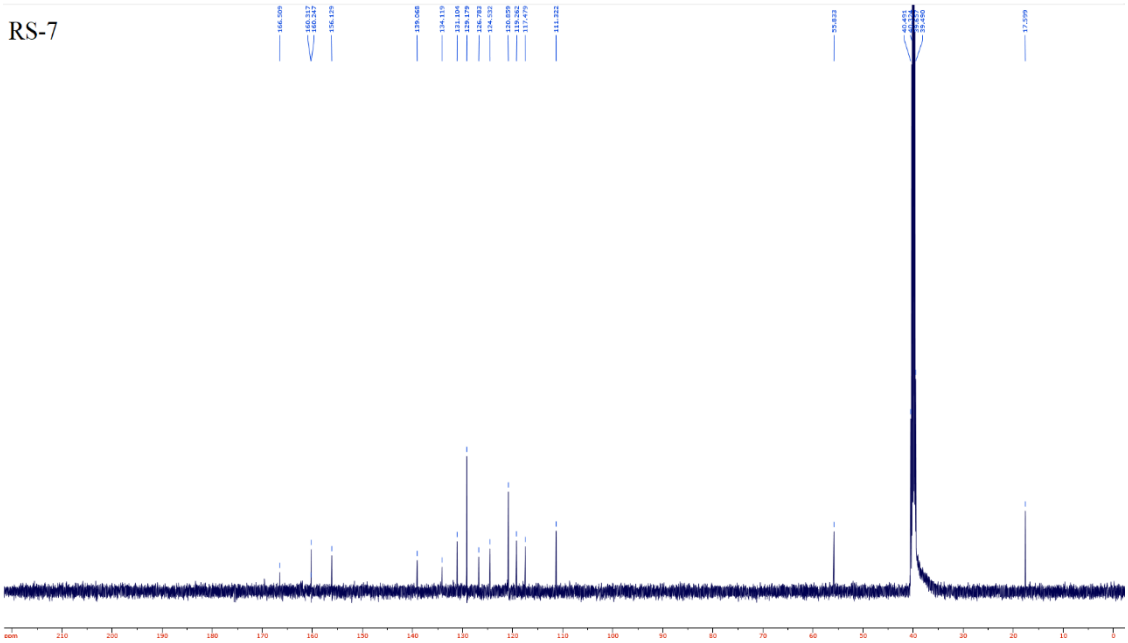

2g

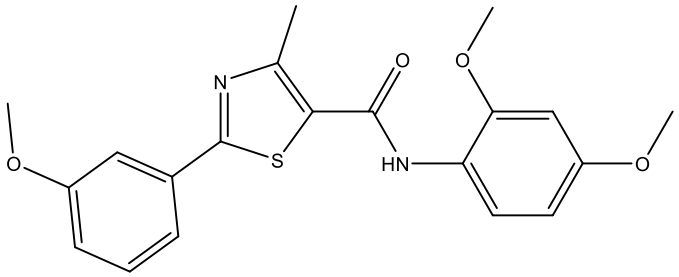

^{1}H-NMR

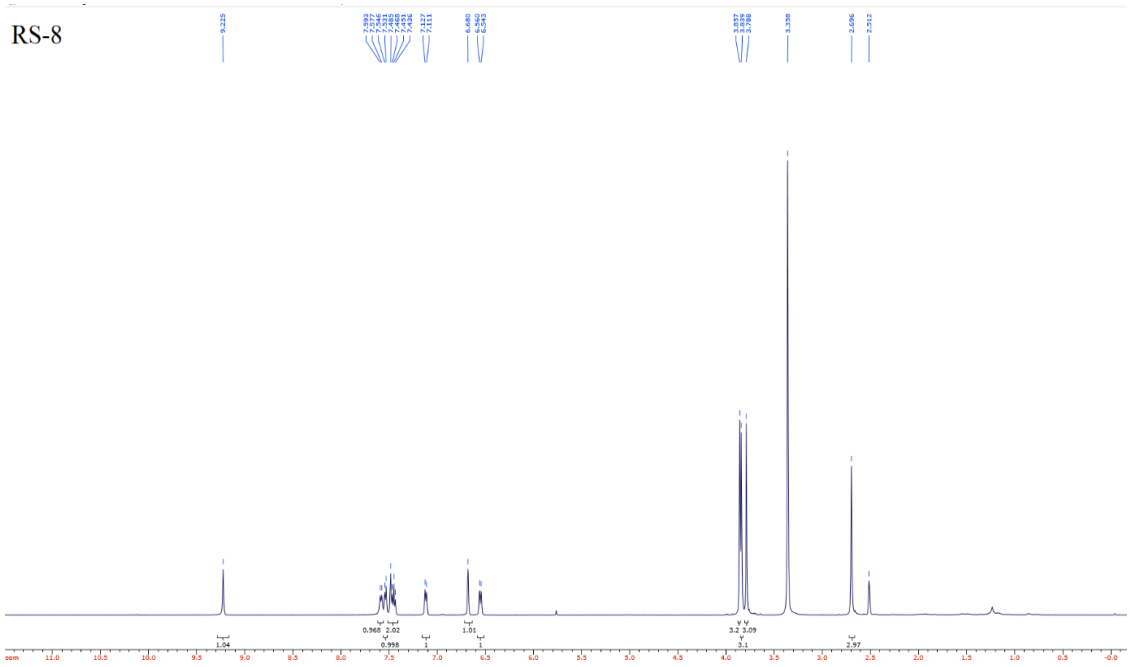

^{13}C-NMR

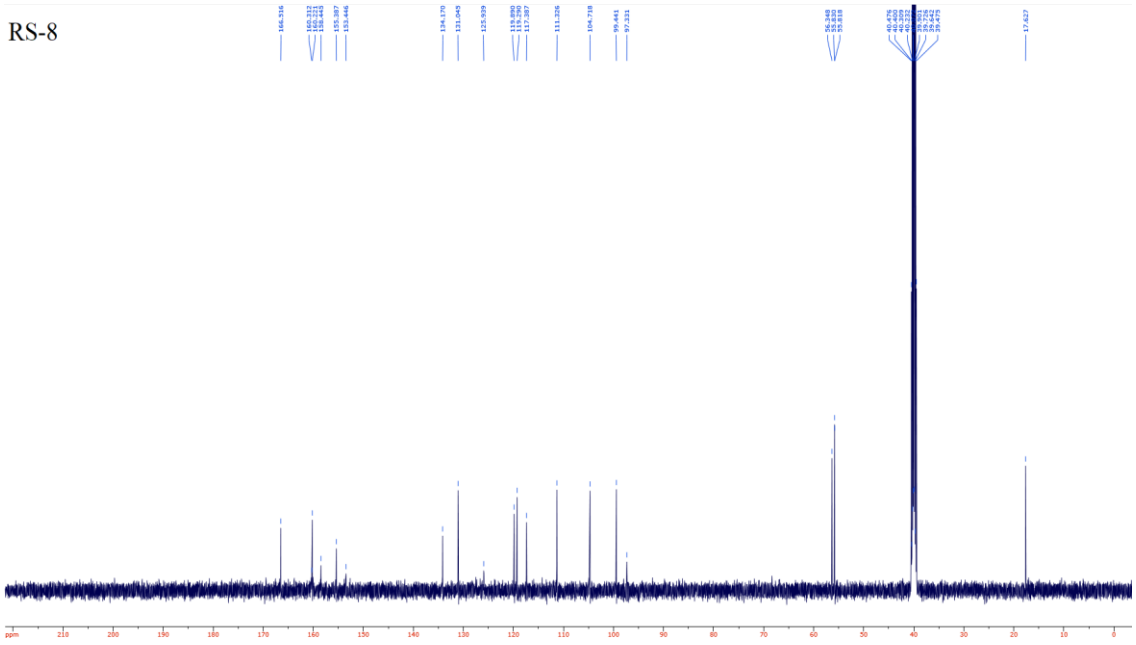

2h

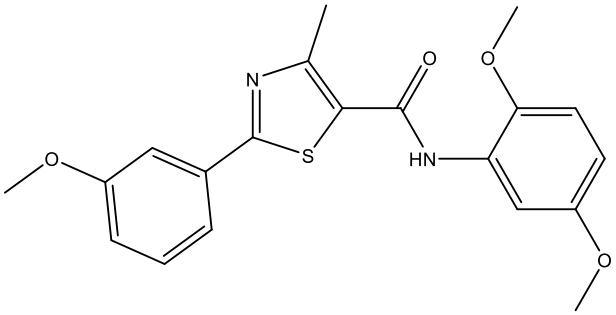

^{1}H-NMR

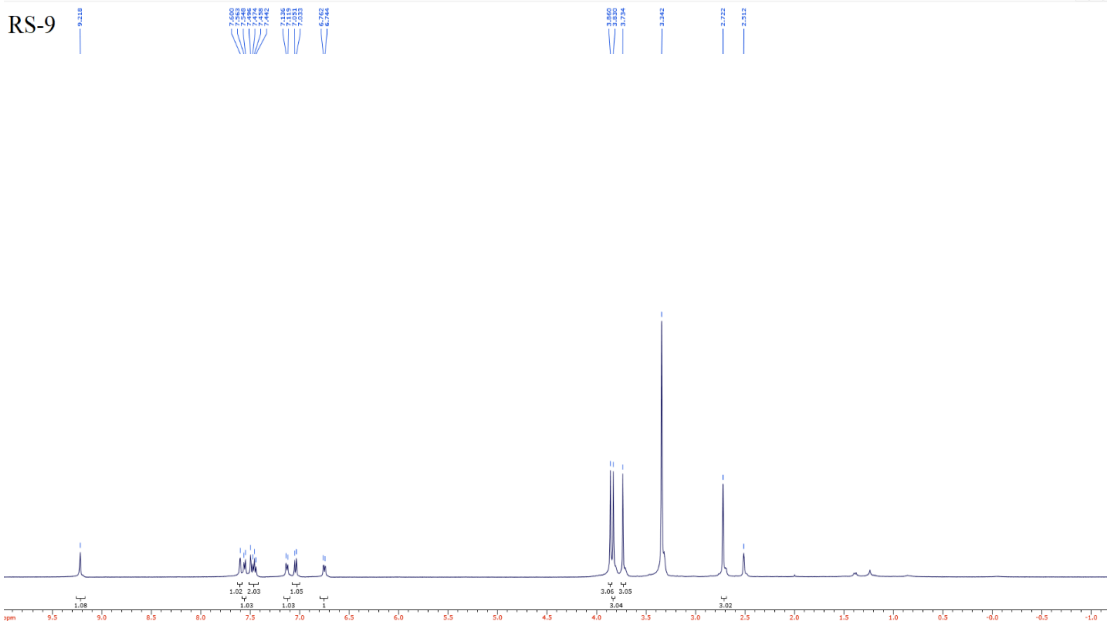

^{13}C-NMR

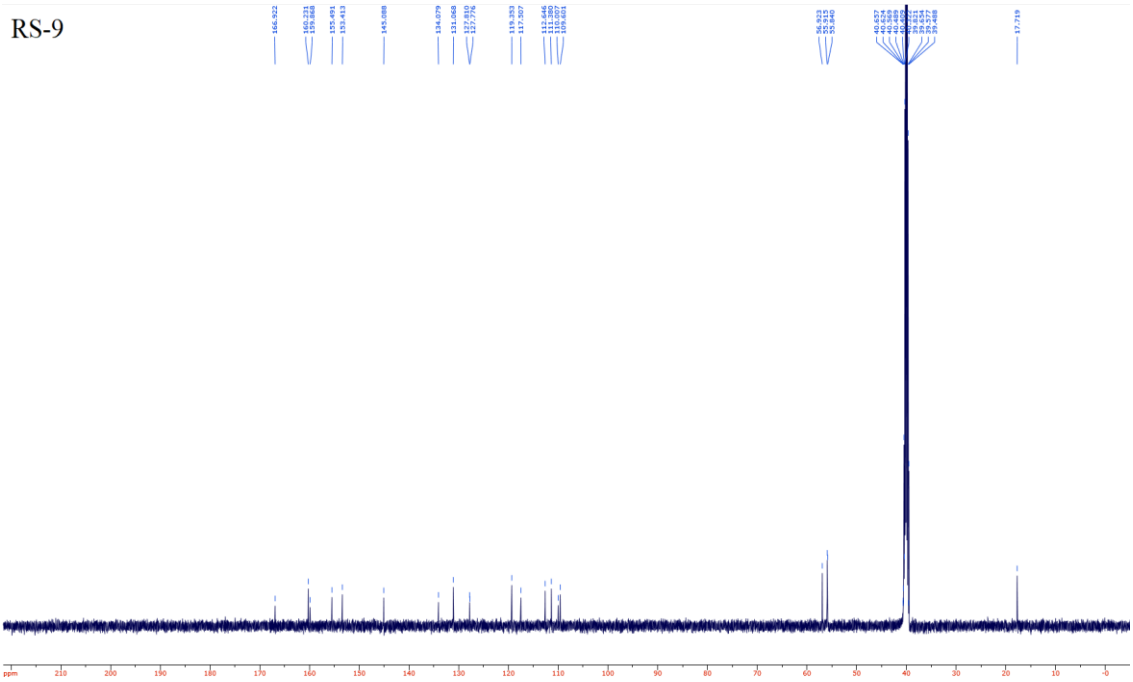

2i

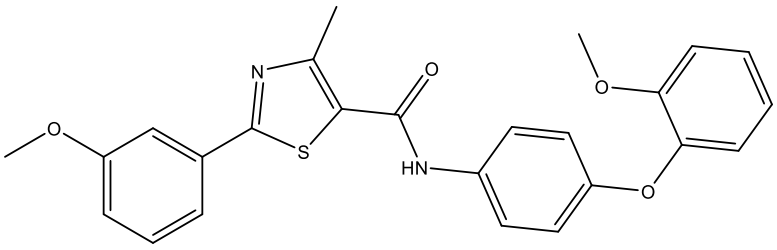

^{1}H-NMR

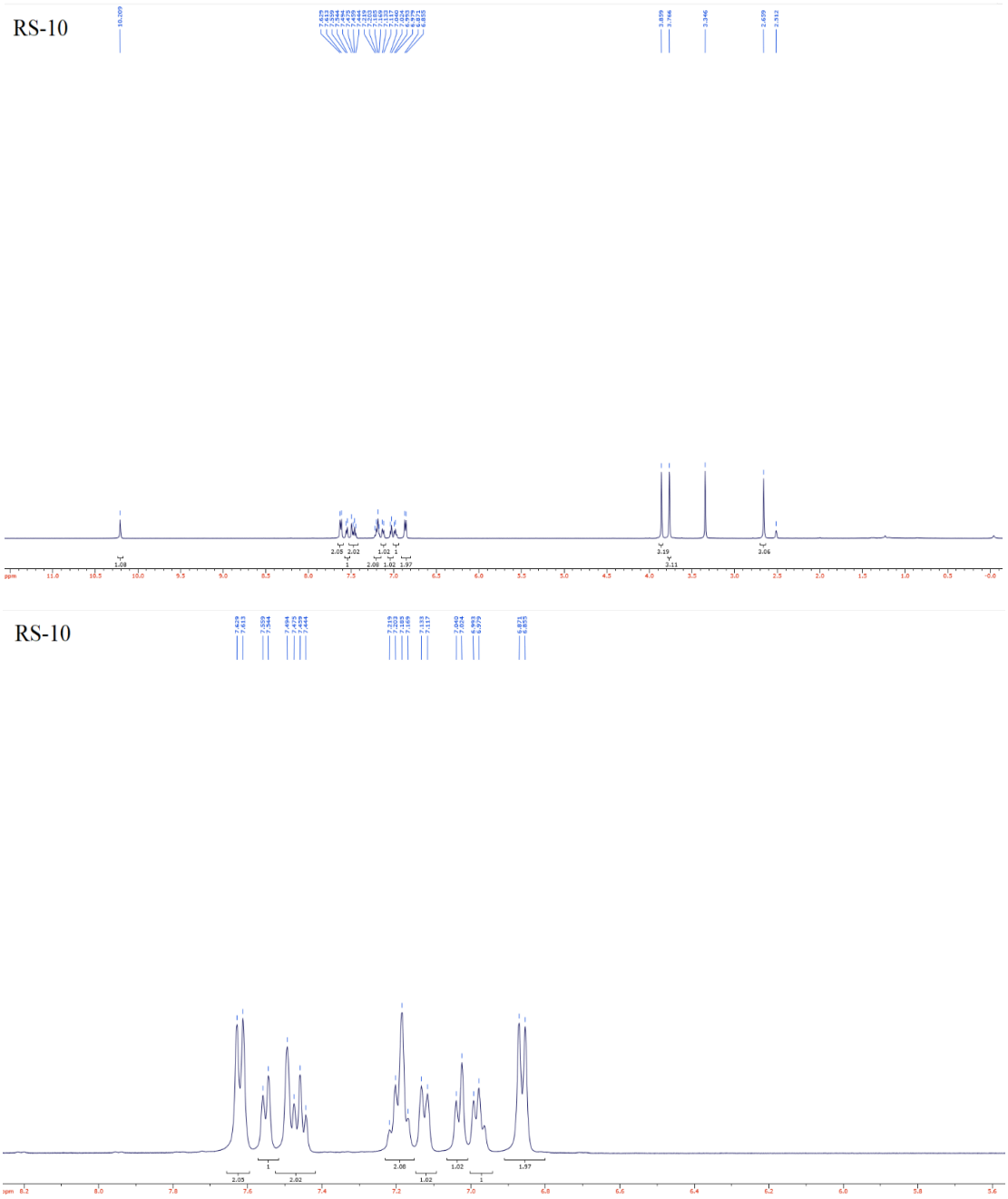

^{13}C-NMR

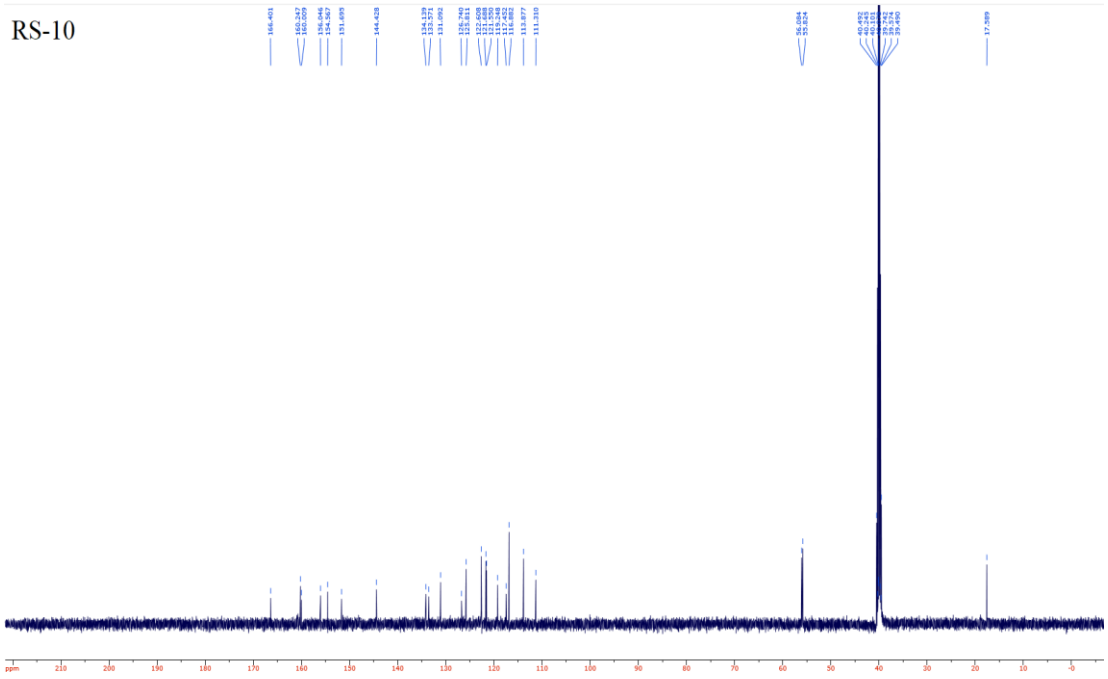

2j

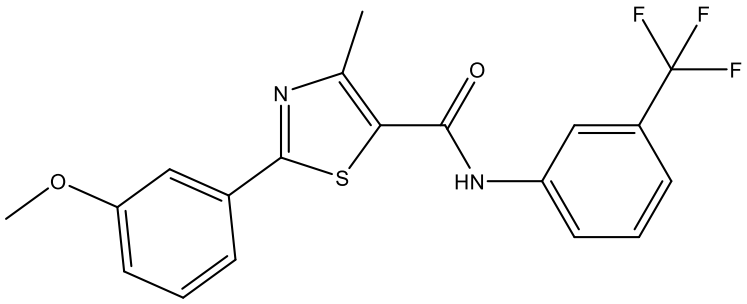

^{1}H-NMR

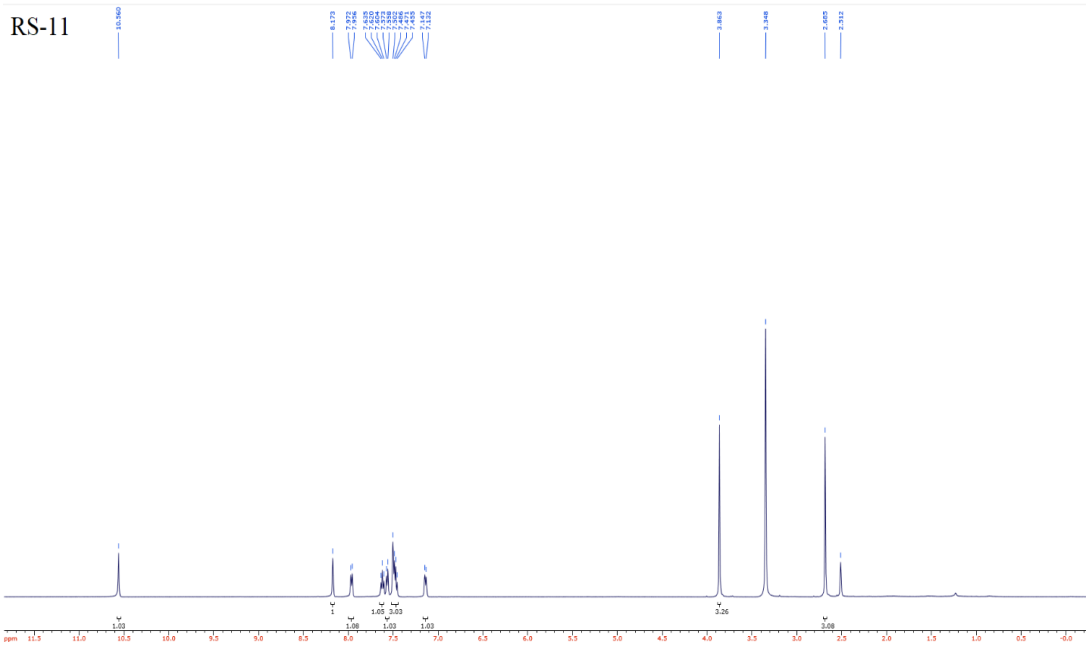

^{13}C-NMR

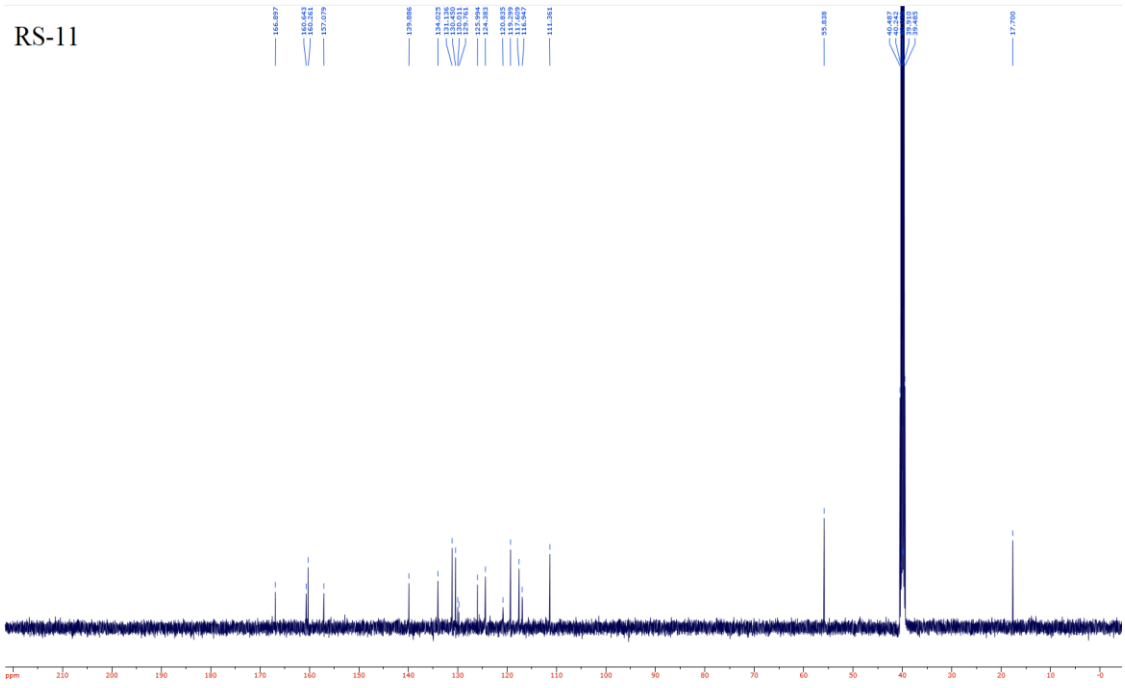

Appendix B

Evaluation for effectiveness of thiazole-carboxamide derivatives compounds on cox-enzymes using two concentrations (5µM and 40µM)

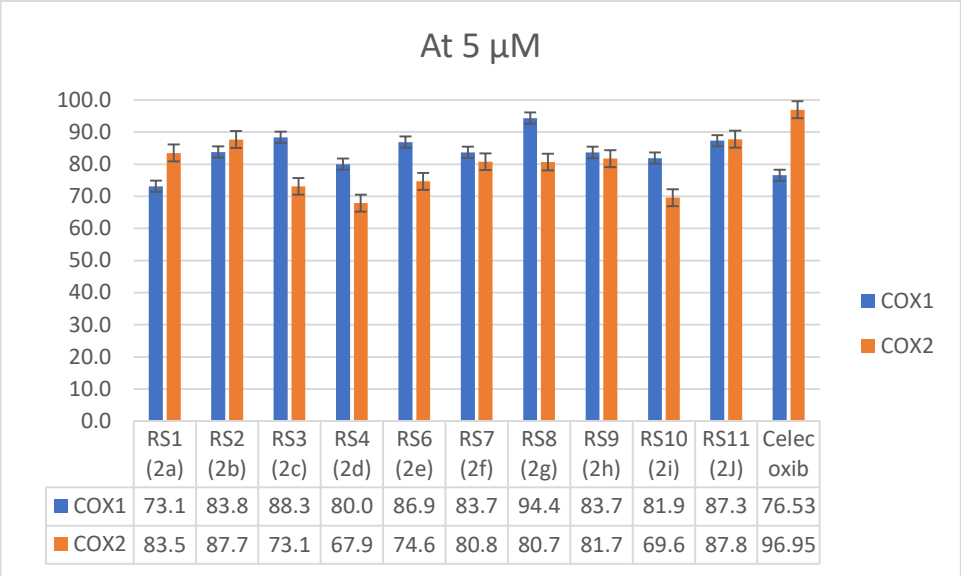

	RS1 (2a)	RS2 (2b)	RS3 (2c)	RS4 (2d)	RS6 (2e)	RS7 (2f)	RS8 (2g)	RS9 (2h)	RS10 (2i)	RS11 (2J)	Celecoxib
COX1	73.1	83.8	88.3	80.0	86.9	83.7	94.4	83.7	81.9	87.3	76.53
COX2	83.5	87.7	73.1	67.9	74.6	80.8	80.7	81.7	69.6	87.8	96.95

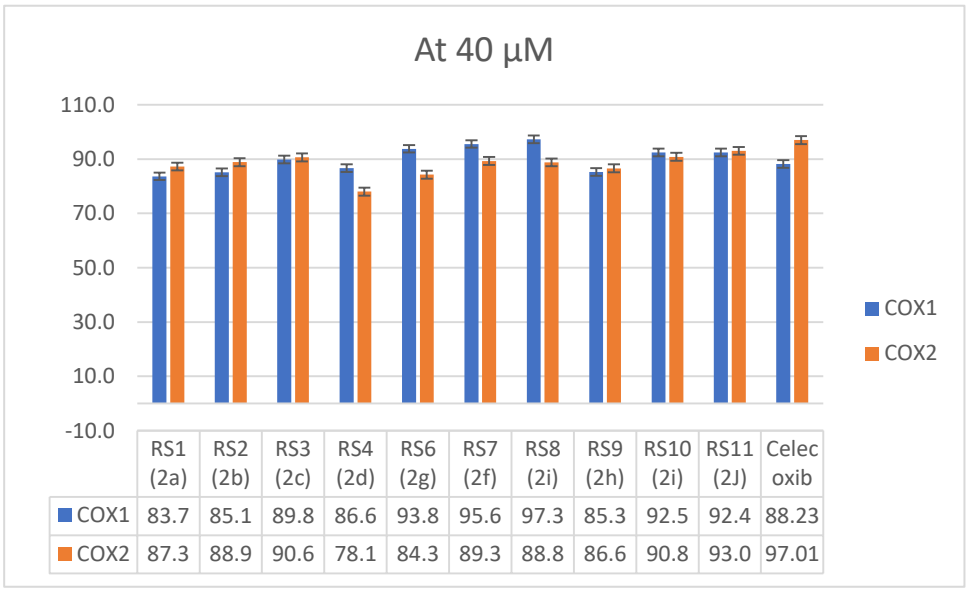

	RS1 (2a)	RS2 (2b)	RS3 (2c)	RS4 (2d)	RS6 (2g)	RS7 (2f)	RS8 (2i)	RS9 (2h)	RS10 (2i)	RS11 (2J)	Celecoxib
COX1	83.7	85.1	89.8	86.6	93.8	95.6	97.3	85.3	92.5	92.4	88.23
COX2	87.3	88.9	90.6	78.1	84.3	89.3	88.8	86.6	90.8	93.0	97.01

جـامعـــة النجاح الوطنية

كليـــة الدراســـات العليـــا

تصميم وتوليف وتقييم بيولوجي لمشتقات ثيازول-كاربوكساميد كمثبطات كوكس

إعداد

روزان غسان سبوبه

إشراف

د. نضال جرادات

د.محمد هواش

قدمت هذه الأطروحة استكمالاً لمتطلبات الحصول على درجة الماجستير في العلوم الصيدلانية، من كلية الدراسات العليا، في جامعة النجاح الوطنية، نابلس- فلسطين.

2022

تصميم وتوليف وتقييم بيولوجي لمشتقات ثيازول–كاربوكساميد كمثبطات كوكس

إعداد

روزان غسان سبوبه

إشراف

د. نضال جرادات

د.محمد هواش

الملخص

العقاقير غير الستيرويدية المضادة للالتهابات (NSAIDs) هي عقاقير تستخدم بشكل شائع لتخفيف الالتهاب وتقليل الألم وخفض درجات الحرارة المرتفعة. إنها تمنع إنزيم الأكسدة الحلقية (COX) المطلوب لتحويل حمض الأراكيدونيك إلى البروستاجلاندين الالتهابي. في أطروحة الماجستير هذه، تم تصنيع مشتقات ثيازول جديدة مع مشتقات الأنيلين وتحديدها وتقييمها من حيث انتقائها وفعاليتها تجاه COX-1 وCOX-2 باستخدام مجموعة اختبار تثبيط كوكس في المختبر. تم تقدير السمية الخلوية للمركبات المركبة باستخدام مقايسة MTS ضد النجم الكبدي البشري (LX-2) بالإضافة إلى خط الخلية الطبيعي (Hek293T). تم تحديد جميع المركبات الجديدة المركبة باستخدام تقنيات HRMS و^{1}H-NMR و^{13}C-NMR. أظهرت النتائج أن المركب الأكثر فعالية ضد إنزيم COX-1 كان b2 مع IC_{50} = 0.2393 ميكرومتر، كما أظهرنشاطا قويا ضد COX-2 مع IC_{50} = 0.1912 ميكرومتر مع نسبة انتقائية (1.2515) . كانت أعلى نسبة انتقائية (2.7661) لمركب a2 مقابل COX-2 مع IC_{50} = 0.958 فيما يتعلق بنسبة السيليكوكسيب (23.8) و IC_{50} ضد COX-2 = 0.002، أظهر مركب j2 أيضًا انتقائية جيده تجاه COX-2 (1.507) مع IC_{50} = 0.957. أظهرت جميع المركبات نشاطًا سامًا للخلايا ضئيلًا ضد خطوط الخلايا الطبيعية التي تم تقييمها وكانت قيم IC_{50} أكثر من 300 ميكرومتر،

باستثناء المركب 2b=1.89 ± 203.71 vlaue IC_{50} و 116.96 ± 2.05 ميكرومتر مقابل خطوط الخلايا LX-2 و Hek293t على التوالي.

الكلمات المفتاحية: إنزيم سيكولوكسيجيناز، مضادات الالتهاب غير الستيرويدية، مضادات الالتهاب، مثبطات كوكس، ثيازول-كاربوكساميد، غير متجانس، دراسات الالتحام.لم تُظهر جميع المركبات نشاطًا سامًا للخلايا على السرطان أو خطوط الخلايا الطبيعية.